Provenance of sandstones in Ethiopia during Late Ordovician and Carboniferous–Permian Gondwana glaciations: petrography and geochemistry of the Enticho Sandstone and the Edaga Arbi Glacials

Anna Lewin[a,]*, Guido Meinhold[b,c], Matthias Hinderer[a], Enkurie L. Dawit[d], Robert Bussert[e]

[a]Institut für Angewandte Geowissenschaften, Fachgebiet Angewandte Sedimentologie, Technische Universität Darmstadt, Schnittspahnstraße 9, 64287 Darmstadt, Germany

[b]Abteilung Sedimentologie / Umweltgeologie, Geowissenschaftliches Zentrum Göttingen, Universität Göttingen, Goldschmidtstraße 3, 37077 Göttingen, Germany

[c]School of Geography, Geology and the Environment, Keele University, Keele, Staffordshire, ST5 5BG, UK

[d]Department of Geology, University of Gondar, P.O. Box 196, Gondar, Ethiopia

[e]Institut für Angewandte Geowissenschaften, Fachgebiet Explorationsgeologie, Technische Universität Berlin, Ackerstraße 76, 13355 Berlin, Germany

*corresponding author. Tel. +49 6151 1620634

E-mail address: alewin@geo.tu-darmstadt.de (A. Lewin).

Abstract

We compare Ethiopian glaciogenic sandstone of the Late Ordovician and Carboniferous–Permian Gondwana glaciations petrographically and geochemically to provide insight into provenance, transport, and weathering characteristics. Although several studies deal with the glacial deposits in northern Africa and Arabia, the distribution of ice sheets and continent-wide glacier dynamics during the two glaciations remain unclear. Provenance data on Ethiopian Palaeozoic sedimentary rocks are scarce. The sandstones of the Late Ordovician glaciation are highly mature with an average quartz content of 95%

and an average chemical index of alteration of 85, pointing to intense weathering and reworking prior to deposition. No evidence for sediment recycling was found. In contrast, the Carboniferous–Permian glaciogenic sandstones are less mature with an average quartz content of 75%, higher amounts of feldspar and rock fragments and a chemical index of alteration of 62. Trace and rare earth element concentrations indicate a higher input of juvenile material, most probably from proximal sources. Comparison with stratigraphically corresponding formations in Saudi Arabia shows similar geochemical patterns for the Upper Ordovician, but major differences in the Carboniferous–Permian. This supports previous assumptions of a large, uniform sediment dispersal system during the Late Ordovician glaciation, in which a combination of long transport paths and exceptionally strong weathering prior to the glaciation produced mature sandstone. During the Carboniferous–Permian, the glacial systems seem to have been more localised and glacial abrasion exposed fresh basement material.

Keywords: Ethiopia, Palaeozoic, glacial sediments, geochemistry, petrography, maturity

1. Introduction

During the amalgamation of the Gondwana supercontinent in the Neoproterozoic (between 650 Ma and 600 Ma before present), the East African Orogen was formed – one of the largest accretionary orogens in Earth's history (Stern, 1994; Collins and Pisarevsky, 2005; Squire et al., 2006). In Northeast Africa, a stable platform developed after the consolidation of the newly formed continent, on which a vast blanket of Palaeozoic sand was deposited (Garfunkel, 2002; Avigad et al., 2005). The sediment transport direction is generally assumed to have been towards the margin of northern Gondwana (e.g., Kumpulainen et al., 2006; Meinhold et al., 2011; Morag et al., 2011). However, the exact provenance of the sediment and its pathways are still poorly understood. Palaeozoic sedimentary rocks in Ethiopia are related to the two major Gondwana glaciations: 1) the Late Ordovician glaciation and the following transgression, probably up to early Silurian and 2) the Carboniferous–Permian glaciation (Saxena and Assefa, 1983; Kumpulainen et al., 2006; Kumpulainen, 2007; Bussert and Schrank, 2007; Bussert, 2010) with a large hiatus between them. Although several studies deal with the glacial deposits in northern Africa and Arabia (Ghienne, 2003; Le Heron et al., 2009; Bussert, 2010; Keller et al., 2011), the distribution of ice sheets and continent-wide glacier dynamics remain unclear. For the Late Ordovician glaciation, a scenario of a large ice sheet covering the whole Sahara region or even whole central Gondwana is proposed (e.g., Ghienne et al., 2007; Le Heron and Craig, 2008). During the Carboniferous–Permian glaciation, a more complex spatial and temporal pattern of ice sheets is likely. Different authors propose a system of several local ice centres, which developed asynchronously across Gondwana (e.g., Eyles, 1993; Fielding et al., 2008). The late Palaeozoic topography in northern Gondwana was influenced by the Hercynian tectonic event and by thermal uplift prior to the formation of the Zagros rift zone that later formed the Neo-Tethys ocean (Sharland et al., 2001). In such elevated areas mountain glaciers may have formed in the Carboniferous–Permian (Konert et al., 2001; Bussert and Schrank, 2007; Le Heron et al., 2009). In southern Libya (Morton et al., 2011) and Saudi Arabia (Knox et al., 2007; Bassis et al., 2016a), provenance changes were identified during the Carboniferous based on heavy minerals, pointing to re-organisation of the sediment dispersal system. A comparative field study on deposits of both Gondwana glaciations in Saudi Arabia was carried out by Keller et al. (2011); detailed petrographic and bulk-rock geochemical data on these formations were provided by Bassis et al. (2016b). Though, in these studies, common glacial and proglacial sedimentary features can be found in both formations, the sedimentary rocks of the Late Ordovician glaciation are significantly more quartzose than those of the late Palaeozoic glaciation. The high maturity of lower Palaeozoic sedimentary rocks of northern Gondwana – untypical for post-orogenic sediment – was also discussed by Garfunkel (2002) and Avigad et al. (2005). Recycling of older sedimentary units cannot be ruled out, but Avigad et al. (2005) suggested strong chemical weathering under a corrosive Cambrian–Ordovician atmosphere in a vegetation-free landscape to be the reason for this high sandstone maturity. Strong chemical weathering is indicated by the highest marine $^{87}Sr/^{86}Sr$ level in Earth's history during that time (e.g., Squire et al., 2006) and may have been enhanced by acidic precipitation due to Ordovician volcanism (Keller and Lehnert, 2010). Morag et al. (2011) assumed a far distant sediment source for lower Palaeozoic sedimentary rocks in Israel and Jordan based on pre-Pan-African detrital zircon ages. In Ethiopia, sedimentological and palynological studies on Palaeozoic glacial successions have been carried out by Dow et al. (1971), Beyth (1972a, b), Saxena and Assefa (1983), Bussert and Schrank (2007), Bussert and Dawit (2009) and Bussert

(2010, 2014), providing evidence that two different glaciations are recorded. Geochemical and heavy mineral data to assess the provenance of these sedimentary rocks are lacking so far. A likely proximal source area is the Arabian–Nubian Shield, which forms the northernmost part of the East African Orogen, and reaches south to the northern Ethiopian basement (Fig. 1). It consists of Neoproterozoic juvenile arcs, younger sedimentary and volcanic basins, voluminous granitoid intrusions, and minor remobilised pre-Neoproterozoic crust and further contains ophiolite (Stern, 1994; Meert, 2003; Johnson et al., 2011; Stern et al., 2012). Potential distal source areas are the Archean cratons and the Proterozoic mobile belts in the centre of Gondwana (Fig. 1).

In this study, we provide petrographic and geochemical data for the two Palaeozoic glaciogenic successions in Ethiopia in order to:

- Differentiate both formations based on petrography and geochemistry making it possible to assign unknown samples to one of them,
- Show that different weathering and transport conditions prevailed during both glacial periods,
- Point out a change in regional correlation with Saudi Arabia (Keller et al., 2011; Bassis et al., 2016a, b) between the two glaciations, reflecting different extents of the palaeo-ice sheets.

2. Geological setting

Palaeozoic sedimentary rocks crop out in the northern Ethiopian province Tigray around the Mekelle Basin and to a minor extent in the Blue Nile region in the west of the country (Fig. 2; Kazmin, 1972; Garland, 1978; Tsige and Hailu, 2007). The Palaeozoic units comprise sediments of the two major Gondwana glaciations in the Upper Ordovician and the Carboniferous–Permian (Saxena and Assefa, 1983; Kumpulainen et al., 2006; Kumpulainen, 2007; Bussert and Schrank, 2007; Bussert, 2010). They overlie Neoproterozoic basement rocks and are in turn overlain by Mesozoic clastic and carbonate sediments (Fig. 2; Beyth, 1972a; Tefera et al., 1996; Dawit, 2010).

The basement in Ethiopia represents the junction of the Mozambique Belt in the south and the Arabian–Nubian Shield in the north (Fig. 1; Kazmin et al., 1978; Tefera et al., 1996; Stern et al., 2012). In the southern part of the Ethiopian basement, Neoproterozoic low-grade metavolcanic and metasedimentary rocks record submarine volcanism and marine sedimentation at the northern rim of the closing Mozambique Ocean (Kazmin et al., 1978; Miller et al., 2003, 2009). In northern Ethiopia, the basement comprises two main units: the metavolcanic/metavolcaniclastic Tsaliet Group and the overlying Tambien Group, a slate and metacarbonate succession, both of up to greenschist facies (Beyth, 1972b; Alene et al., 2006). Syn- and post-tectonic granites and diorites intruded both units (Beyth, 1972b; Kazmin et al., 1978; Tefera et al., 1996).

The Palaeozoic glacial deposits of Ethiopia were first described by Dow et al. (1971) and Beyth (1972a, b) as two facies (tillite facies –

Edaga Arbi Glacials and sandstone facies – Enticho Sandstone), which interfinger laterally and both, in places, lie unconformably on the basement. They assigned both facies to one glacial episode. Later, early Palaeozoic trace fossils (e.g., *Arthrophycus alleghaniensis*) were found in the upper part of the Enticho Sandstone and gave a minimum age for the underlying glaciogenic deposits (Saxena and Assefa, 1983; Kumpulainen et al., 2006; Bussert and Dawit, 2009). In the Edaga Arbi Glacials, Carboniferous–Permian palynomorphs provide age control (Bussert and Schrank, 2007; Bussert, 2014).

The Enticho Sandstone unconformably overlies the Neoproterozoic basement and has a thickness of up to 200 m (Saxena and Assefa, 1983; Dawit, 2010). Bussert and Dawit (2009) provide detailed facies descriptions. It consists of basal tillite, a lower glaciogenic sandstone unit and an upper shallow marine sandstone unit. The tillite is exposed only in the area east of Wukro (Fig. 2). Its matrix is red medium sand. Clasts are angular boulders of metavolcanics, metapelites and conglomerates, probably from the local basement, and well-rounded quartz pebbles, which may be recycled (Fig. 3g). Since large volumes of sandstone are not present in the local basement, the matrix material may have been transported from further away. Associated with the tillite are soft sediment deformation structures in underlying sandstone (Fig. 3h) and in the tillite itself, which may represent shallow marine push-moraine or grounding line complexes (Dawit, 2010). The glaciogenic unit consists mainly of massive, partly large-scale cross-bedded fine- to medium-grained sandstone, with intercalated gravel beds (Fig. 3f) interpreted to represent pulses of glacial outwash (Bussert and Dawit, 2009). The shallow marine unit comprises well-sorted sandstones with bipolar cross-bed sets and rhythmic mud drapes suggesting a tide-dominated shallow marine depositional setting (Fig. 3d, e; Bussert and Dawit, 2009; Dawit, 2010). The Enticho Sandstone occurs along the eastern rim of the Mekelle Basin (Fig. 2a).

The Edaga Arbi Glacials unconformably overlie the Enticho Sandstone and, in places, lie directly on the basement (e.g., Beyth, 1972b). They crop out along the western and south-western margin of the Mekelle Basin and to a minor extent in the Blue Nile region in western Ethiopia (Fig. 2). Their thickness is approximately 200 m in northern Ethiopia, but significant lateral thickness variations occur (Bussert, 2010). Bussert and Dawit (2009) and Bussert (2014) give detailed descriptions of the sediment facies. The Edaga Arbi Glacials consist of tillite at the base overlain by laminated clay- and siltstones, which contain scattered out-sized clasts and lenses of sandstone (Fig. 3a; Beyth, 1972b; Bussert and Dawit, 2009; Bussert, 2014). In the tillite, mostly rounded boulders of granitoid, metabasic and metasedimentary rocks are found and often exhibit striated surfaces (Fig. 3c). Outsized clasts in rhythmic lamination of sandstone and silt- to claystone (Fig. 3b) are interpreted as dropstones (Bussert and Dawit, 2009; Bussert, 2014). The sandstone lenses may represent channelized glacial outwash deposits or hyperpycnal sediment flows (Bussert and Dawit, 2009; Bussert, 2014). Bussert (2014) proposed a model for the generation of this succession with initial glacier advance and the deposition of tillites, followed by the formation of subaerial and subaqueous outwash fans during the glacier retreat and the final suspension settling of silt and clay in calm water of a proglacial lake or fjord. Periodic hyperpycnal sediment flows and the deposition of dropstones interrupted the suspension settling. The association of the Edaga Arbi Glacials with glacial landforms on the basement surface, such as roche moutonnées, rock drumlins, as well as glacial striae, confirms a glacial origin (Bussert, 2010). In the Blue Nile region (Fig. 2b) Permian–Triassic continental sandstones partly overlie the Edaga Arbi Glacials (Dawit, 2014).

The Palaeozoic succession is – unconformably in northern Ethiopia – overlain by the Mesozoic Adigrat Sandstone, the Antalo Limestone, Agula Shale and Amba Aradam Formation (Beyth, 1972b; Dawit, 2010).

3. Sampling and methods

Thirty-two sandstone samples were taken from surface outcrops, 19 from the Enticho Sandstone and 13 from the Edaga Arbi Glacials. The focus of the sampling campaign was on northern Ethiopia since Palaeozoic glacial sediments are more abundant there. In the Blue Nile region in the west of the country, glacial sediments could be identified at only one locality (Fig. 2b). In addition to the sedimentary rocks, seven samples from the local basement of northern Ethiopia were studied, as well as 11 samples from boulders in tillite of the Edaga Arbi Glacials. Fig. 2 shows the sample locations; Table 1 provides the corresponding coordinates. Sampling sites were chosen in order to cover a laterally extensive area based on previous stratigraphic and sedimentological work of R. Bussert and E. L. Dawit (Bussert and Schrank, 2007; Bussert and Dawit, 2009).

We paid attention to select sampling sites where there is biostratigraphic control on the sediments. Furthermore, we distinguished the Enticho Sandstone and Edaga Arbi Glacials based on homo-/heterogeneity in grain size and mineralogy, and on sedimentary structures: The outcrops of the Enticho Sandstone – apart from the tillite at the base of one outcrop (see Section 2 in this paper) – appear uniform in grain size and mineralogy (highly quartzose). The Edaga Arbi Glacials are much more heterogeneous (see Section 2). In the Edaga Arbi Glacials, we mainly sampled from the sandy lenses. Three samples are from the tillite matrix (Table 1). One sample was taken with highly uncertain stratigraphic assignment (sample Eda-5, Table 1). For reasons of comparability, we focused on the fine-grained parts of the sandstones during sampling, i.e. a dominating grain size of 63–250 µm, using the grain-size comparator chart for field work by Stow (2005).

3.1. Petrography

Thin sections were prepared from all samples. The samples from the basement and the tillite boulders were studied only qualitatively to determine the rock type. The framework composition of the sandstone samples was assessed by point-counting of 300 grains per sample using the "traditional" counting method (e.g., Decker and Helmold, 1985). In contrast to the Gazzi-Dickinson method (e.g., Ingersoll et al., 1984; Zuffa, 1985), minerals within lithic fragments are counted as the type of fragment they occur in. We used this method to make sure that information conveyed by the type of lithic fragment is not lost. However, only few lithic fragments are present in the samples so that the choice of the counting method does not have a significant effect on the result. The matrix content was estimated based on the comparison chart of Folk (1951) with an upper grain-size limit for the matrix of 30 µm. Sorting and roundness of the framework grains were estimated according to Powers (1953). For sandstone classification, we used the scheme of McBride (1963; Fig. 4). We did not use the scheme of Dott (1964) that includes wackes, even though many samples have a high matrix content (Table 2). This is, because in many cases it cannot be decided whether the matrix is primary or secondary.

3.2. Major and trace element geochemistry

For geochemical analysis, ~50 g of each of the 50 samples were pulverised to a particle size <63 µm using an agate vibratory disc mill. Geochemical analyses were carried out at the Geoscience Centre at the University of Göttingen, Germany. Concentrations of major elements and selected trace elements were determined by X-ray fluorescence analysis (XRF) on fusion tablets. For each sample, 2.8 g of rock powder were mixed with 5.6 g of a di-lithium tetraborate/lithium metaborate fluxing agent (Spectromelt® A12, Merck) and 0.64 g lithium fluoride and fused in platinum crucibles at 1250 °C. XRF analysis was performed using a PANalytical AXIOS Advanced sequential X-ray fluorescence spectrometer equipped with a rhodium target tube for sample excitation and the software SuperQ 4 for data processing. Further trace elements, including rare earth elements (REE), were quantified using inductively coupled plasma mass spectrometry (ICP-MS) on the dissolved sample. For each sample, 100 mg of rock powder were digested in the following steps using a PicoTrace® acid sample digestion system: (1) pre-reaction with 2 ml HNO_3 at 50 °C overnight, (2) first pressure phase with 3 ml HF (40%) and 3 ml $HClO_4$ (70%) at 150 °C for 8 hours, (3) evaporation at 180 °C for 16 hours, (4) second pressure phase with 10 ml double de-ionised water, 2 ml HNO_3 and 0.5 ml HCl at 150 °C for 4 hours. The resulting solution was diluted to 100 ml with ultrapure water. Analysis was performed using a ThermoElectron VG PlasmaQuad 2 quadrupole ICP-MS. Measurements were calibrated to the standard JA-2 of the Geological Survey of Japan.

The Eu anomaly of the sandstone samples was calculated as suggested by McLennan (1989):

$$\frac{Eu}{Eu^*} = \frac{Eu_N}{(Sm_N * Gd_N)^{0.5}}$$

The subscript *N* indicates chondrite-normalised values (see Fig. 6).

To put the degree of weathering and leaching into numbers, we calculated the frequently used chemical index of alteration, as proposed by Nesbitt and Young (1982):

$$CIA = \frac{Al_2O_3}{(Al_2O_3+CaO^* +Na_2O+K_2O)} * 100.$$

The molecular proportions of the respective oxides are used. CaO* is the amount of CaO incorporated in silicates. Therefore, out of the Edaga Arbi Glacials only five samples without carbonate cementation are considered. To get an idea of the tectonic signature of the sandstones we used the tectonic setting discrimination diagrams of Verma and Armstrong-Altrin (2013, 2016) based on discriminant functions employing major oxides and trace elements.

For statistical analysis of the data, their compositional nature – vectors of non-negative values summing up to a whole – was taken into account. Standard multivariate statistical methods are designed for data in the real space whereas the sample space of compositional data is the simplex with the respective dimension (Aitchison, 1982; Egozcue et al., 2011). To transform compositional data from the simplex to the real space, Aitchison (1986) introduced the principle of log-ratio transformation, that is, taking the logarithms of ratios of components. In this study, we used the centred log-ratio (clr) transformation to perform a principal component analysis (PCA) of the major and trace element data. This means that parts of a composition (e.g., element concentrations of a sample) are transformed by taking the natural logarithm of the ratio of the respective part and the geometric mean of the whole composition (Aitchison, 2003). We performed a second PCA not considering the highly mobile elements K, Rb, Ba, Sr, Mn, and Na. The high variability of these elements masks the provenance signal. Moreover, Ca and Mg are excluded, because they are probably influenced by carbonate cement. The major and trace element data of the local basement and tillite boulders were used for comparison. For the use of log-ratios, the data set must not contain any zeros. Therefore, those have to be replaced by small values. We chose a multiplicative zero replacement using 0.65 times the detection limit, as suggested by Martín-Fernández et al. (2003), since only very few values are below the detection limits of the XRF and ICP-MS.

4. Results

4.1. Petrography

According to the classification scheme of McBride (1963; Fig. 4) the glaciogenic facies of the Enticho Sandstone is quartzarenite to subarkose with an average composition of 90.5% quartz, 7.4% feldspar and 1.4% lithic fragments. The marine facies is quartzarenite with an average composition of 99.0% quartz, 0.2% feldspar and 0.3% lithic fragments (Fig. 4, Table 2). The lithic fragments are mostly plutonic or sedimentary. The sedimentary lithoclasts are fine sand- to siltstone, sometimes with metamorphic overprint, indicated by foliation. As expected, grain size and roundness are more variable in the glaciogenic than in the marine unit (Fig. 5b, c, Table 2). The average matrix content is 16% with an average in the glaciogenic unit of 20% and 11% in the marine unit. Accessory minerals are mostly zircon, tourmaline, rutile, and some opaque phases. The sandstones in the Edaga Arbi Glacials are subarkose to arkose with an average composition of 74.8% quartz, 18.9% feldspar and 3.3% lithic fragments (Fig. 4, Table 2). Most lithic fragments are plutonic or sedimentary, as in the Enticho Sandstone, but few volcanic lithics were also counted (Table 2). Apart from zircon, tourmaline, rutile, and opaque phases, garnet is an additional accessory mineral. The sandstones in the Edaga Arbi Glacials are generally heterogeneous in composition and texture with variable roundness and moderate sorting (Fig. 5a, Table 2). The average matrix content is 20%. Four of 13 analysed samples of the Edaga Arbi Glacials are strongly cemented with calcite with 20–25% of the thin section area, four samples contain up to 5% calcite cement and the remaining five samples contain almost no calcite. No indicators for significant sediment recycling, such as abraded quartz overgrowths or abundant sedimentary lithoclasts, were found in either of the two formations.

The samples taken from the basement include two metagreywackes, one metatillite, one metapelite, one metabasite, and two granites. The boulders sampled from the tillite at the base of the Edaga Arbi Glacials are classified as six granitoids, two diorites/gabbros, two metabasites, and one paragneiss (Table 1).

4.2. Bulk-rock geochemistry

The Enticho Sandstone, especially the marine unit, is depleted in the mobile elements Rb, Ba, K, and Sr but enriched in Th and Zr compared to the average upper continental crust (Fig. 6). Its elemental composition is highly variable, especially in the mobile elements. The REE pattern is typical for sedimentary rocks of upper crustal origin (Fig. 6; McLennan et al., 1993). The chondrite-normalised La_N/Yb_N, which quantifies the LREE enrichment, is on average 10.7 (Appendix). The Eu anomaly is pronounced (i.e. <1) in the Enticho Sandstone with a mean Eu/Eu* for the glaciogenic facies of 0.8 and 0.7 for the marine facies. The CIA is on average 92 for marine facies and 78 for the glaciogenic facies (Appendix). The elemental composition of the Edaga Arbi Glacials is more uniform. The depletion in mobile elements and the Zr enrichment is less than for the Enticho Sandstone. The chondrite-normalised La_N/Yb_N is on average 5.9 and the mean Eu/Eu* 0.9. The average CIA is 62 (Appendix). Sample Eda-5, with uncertain stratigraphic assignment, differs from the Edaga Arbi Glacials sandstone by high depletion in mobile elements, Zr enrichment, and a high CIA of 95 (Fig. 6; Appendix).

In the PCA biplot of major and trace elements (Fig. 7a), a clear separation between the two formations as well as between the glaciogenic and the marine facies becomes obvious: along the rays of Ni and Th (enriched in Enticho Sandstone) versus Ca, Mg, and Na (enriched in Edaga Arbi Glacials) the two formations can be distinguished. Along the rays of K, Rb, Ba, and Sr (enriched in glaciogenic) versus P, Y, V, Sc, and HREE (enriched in marine), different facies separate. Sample Eda-5 has a similar composition to the Enticho Sandstone. The first three principal components (Fig. 7b, c) of the PCA excluding mobile elements and carbonate cement influence together explain 74% of the total variability. Again, a separation of the two formations is possible with the Enticho Sandstone being enriched in Th, Zr, Hf, U, and Si and depleted in P and Al compared to the Edaga Arbi Glacials. This separation is facies-independent since no clustering of marine and glaciogenic Enticho Sandstone is visible. No patterns related to stratigraphic or geographic sampling position were detected (not shown in Fig. 7).

In the tectonic setting discrimination diagram of Verma and Armstrong-Altrin (2013) based on major oxide concentrations, the Enticho Sandstone plots in the “continental rift” field, the Edaga Arbi Glacials in the “continental rift” and “collision” fields (Fig. 8a). In the active versus passive margin diagram of Verma and Armstrong-Altrin (2016; Fig. 8b) based on major oxides and selected trace elements, the Enticho Sandstone is assigned to a passive margin setting whereas the Edaga Arbi Glacials plot partly in the active and partly in the passive margin field. The Th/Sc and Zr/Sc ratios are generally higher for the Enticho Sandstone than for the Edaga Arbi Glacials (Fig. 9). Significant Zr enrichment that would lead to a deviation from the compositional trend is not clearly visible for either of the formations. A plot of the Th/Sc versus Zr/Sc ratios of the samples grouped geographically into north, centre, and south (Fig. 9b) reveals a trend towards higher Th/Sc and higher Zr/Sc ratios along the assumed transport direction from south to north for both formations.

Of the basement samples, the granites are enriched in Nb, HREE, and Y and depleted in Cr and Ni compared to the centre of the data set plotted in Fig. 10. The metasediments are enriched in V, Sc, Fe, Ni, and Cr and depleted in Zr, Th, Hf, and U, similar to the metabasite (Fig. 10). The overall composition of the basement samples resembles that of the Edaga Arbi Glacials (Fig. 10). Of the boulders sampled from tillite at the base of the Edaga Arbi Glacials, the granitoids have similar compositions to the granites in the basement (Fig. 10a). The diorites/gabbros have variable compositions, one being rich in P and the other in Fe and Sc (Fig. 10). Of the basalts, one is enriched in HREE, Nb and Y, the other in V, Sc, and Cr. The composition of the paragneiss is close to the centre of the data set with slight enrichment in Fe, Sc, and Cr.

5. Discussion

When interpreting bulk-rock geochemical data, grain-size effects have to be considered (e.g., Rollinson, 1993; von Eynatten et al., 2012). The grain-size distribution of a sediment is influenced by transport processes, such as hydraulic sorting and comminution (e.g., Rubey, 1933; Garzanti et al., 2008; von Eynatten et al., 2012), and by the inherited grain size of the respective mineral in the parent rock (Morton and Hallsworth, 1994). Even though we collected samples of the same major grain size, the degree of sorting of framework grains and the matrix content differ (Section 4; Table 2). Therefore, for instance, the high contents of Mg, Ca, Na, and K in the glacial samples (Fig. 7a) are probably not only related to (little) weathering and (strong) diagenesis but also to the poor sorting and higher matrix content of the glacial samples as compared to the marine (Table 2). To account for the facies differences, we plotted the glaciogenic and marine facies of the Enticho Sandstone separately in the respective diagrams (Fig. 4, Fig. 6-10).

A clear distinction of the two formations is possible, particularly in terms of their major and trace element compositions (e.g., Figs. 7, 8). This makes it possible to assign stratigraphically uncertain samples: Sample Eda-5 was tentatively assigned to the Edaga Arbi Glacials by sedimentological characteristics in the field but without biostratigraphic evidence. Based on the geochemical characteristics it is likely that it belongs to the Enticho Sandstone instead. Furthermore, the samples taken from an outcrop in Enticho (samples Eda-2 and Eda-3; Table 1) – originally the type location of the Enticho Sandstone – can be assigned to the Edaga Arbi Glacials based on their petrography and chemical composition (Table 2, Appendix).

The high variability in Ca, Mg, Na, K, Rb, and Ba (Fig. 7a) in the data set reflects the high mobility of these elements, which are present in the glaciogenic sedimentary rocks but leached from the marine. The enrichment of Si in the Enticho Sandstone (Fig. 7) indicates a higher quartz content, which is in agreement with petrographic observations (Fig. 4, Table 2) and points to high maturity. The negative correlation of Al and Si (Fig. 7b) indicates transport processes that remove clay minerals and feldspars and destroy lithic fragments, and thus relatively enrich quartz in the Enticho Sandstone. Similarly, the negative correlation of P and Th (Fig. 7b, c) suggests weathering under acidic conditions, in which apatite is destroyed and Th persists, and which affected the Enticho Sandstone more than the Edaga Arbi Glacials. This is supported by the higher CIA values for the Enticho Sandstone (Appendix). The correlations of Hf, Th, U, and Nb with Zr and Ti in the Enticho Sandstone (Fig. 7) suggests that these elements are carried zircon and rutile. The presence of these stable heavy minerals is an additional indicator for maturity. The high maturity of the Enticho Sandstone is probably a consequence of (1) intense chemical weathering in the source area prior to the glaciation and (2) long transport and/or marine reworking, in which clay minerals produced during weathering are removed from the sediment. Intense chemical weathering in northern Gondwana under a corrosive Neoproterozoic to pre-glacial Ordovician atmosphere was suggested by, e.g., Avigad et al. (2005). The assignment of the Enticho Sandstone to “continental rift” and “passive margin” settings based on major and trace element composition (Fig. 8; Verma and Armstrong-Altrin, 2013, 2016) is related to the higher maturity as well.

For the Edaga Arbi Glacials, on the other hand, Al enrichment indicates a higher content of feldspar and clay minerals and thus a lower maturity (Fig. 7b, c). Since Eu is enriched in plagioclase, the less pronounced Eu anomaly in the Edaga Arbi Glacials (Fig. 6) corresponds to a higher feldspar content as well. This is in accordance with the petrographic observations (Fig. 4, Table 2). The higher concentration of HREE in the Edaga Arbi Glacials is probably related to the presence of garnet. The tendency of the Edaga Arbi Glacials to “collision” and “active margin” signatures (Fig. 8) points to fresher, less reworked material deposited in the Carboniferous–Permian and does not have to indicate different tectonic settings.

Neither petrography nor the Th/Sc and Zr/Sc ratios give hints to sedimentary recycling being an important process for one of the formations. The few fine-grained and foliated sedimentary lithoclasts may be due to local erosion of slates from the Neoproterozoic basement. The south-north trend of Th/Sc and Zr/Sc ratios in both formations (Fig. 9b) may be due to progressive enrichment of stable heavy minerals, such as zircon, along the transport path. Zircon is a major carrier of Zr and Th (Fig. 7). Another possibility would be the admixture of felsic material.

The enrichment of the Enticho Sandstone in Zr, Hf, Th, U, Nb, and the light REE (Figs. 6, 7) points to felsic source rocks. The pronounced negative Eu anomaly (Fig. 6) indicates evolved crustal material as a source. Possible source areas are the Archean cratons

(Congo Craton, Tanzania Craton) or the Proterozoic mobile belts (Kibaran Belt, Irumide Belt, Mozambique Belt) in the inner part of Gondwana (Fig. 1). A distal source area in central Gondwana was also proposed for Cambrian–Ordovician sandstone in Israel and Jordan: Based on detrital zircon ages, Kolodner et al. (2006) inferred a progressive southward migration of the source area during the Cambrian–Ordovician. Hf isotopic data of Neoproterozoic zircons from these formations are incompatible with the local Arabian–Nubian Shield. This led Morag et al. (2011) to the assumption that the source region might be within the remobilised crustal areas further south (Fig. 1). If this trend extends to the Upper Ordovician, a distal source area in the inner part of Gondwana for the Enticho Sandstone is likely.

In the Edaga Arbi Glacials, the relative enrichment of V and Cr and the higher proportion of HREE indicates a higher influence of mafic and garnet-bearing source material (e.g., Bhatia and Crook, 1986; McLennan et al., 1993). For example, smectite – commonly a weathering product of mafic precursor minerals – can be rich in Cr and V (e.g., Chamley et al., 1979). Garnet is a major carrier of HREE (e.g., Harangi et al., 2001). The poor Eu anomaly (Fig. 6) indicates contribution of juvenile source material (McLennan et al., 1993). Similarly, the lower Th/Sc of the Edaga Arbi Glacials compared to the Enticho Sandstone points to a higher influence of undifferentiated crustal material (Fig. 9; McLennan et al., 1993). A proximal source area composed mainly of juvenile crust would be the Arabian–Nubian Shield, which is the northernmost edge of the East African Orogen (Johnson et al., 2011). Ophiolites in the Arabian–Nubian

Shield, as described for instance by Meert (2003), Johnson et al. (2011), and Stern et al. (2012), could be the source for mafic input in the Edaga Arbi Glacials. Volcanic rock fragments in the Edaga Arbi Glacials may indicate late Palaeozoic volcanism, as speculated by Sacchi et al. (2007). However, it cannot be said with certainty that the rock fragments are not metamorphically overprinted and older. Metavolcanic rocks are abundant in the Neoproterozoic basement and are a likely source for these fragments. The similar overall composition of the local basement samples and the Edaga Arbi Glacials (Fig. 10) supports the assumption of a local source for these and a different source area for the Enticho Sandstone.

Petrographic and chemical compositions of glacial successions of Upper Ordovician and Carboniferous–Permian sandstone in Saudi Arabia are similar to those obtained in Ethiopia: a signature of old crustal material in the early Palaeozoic and a higher influence of juvenile material in the late Palaeozoic (Bassis et al., 2016b). In the PCA biplot (Fig. 10), however, the Carboniferous–Permian samples from Saudi Arabia plot far away from the corresponding samples of this study, whereas the Upper Ordovician samples are grouped with the corresponding. Therefore, for the early Palaeozoic a common provenance for the glacial sandstones of both areas is likely, whereas in the late Palaeozoic the sediments were probably supplied from different local sources (Fig. 11). This supports the assumption of a large North Gondwana ice sheet in the Late Ordovician (Ghienne et al., 2007; Le Heron and Craig, 2008) and more local glacial systems during the Carboniferous–Permian glaciation (Eyles, 1993; Fielding et al., 2008).

Conclusions

The petrographic and geochemical comparison of sandstones deposited during the two Gondwana glaciations in the Late Ordovician and the Carboniferous–Permian reveals clear differences. The Upper Ordovician Enticho Sandstone is highly mature with a major and trace element composition typical for old differentiated crustal provenance. In contrast, the sandstone of the Carboniferous–Permian Edaga Arbi Glacials is less mature with a geochemical signature of more juvenile source material. Its major and trace element composition resembles that of the local basement. Stratigraphically equivalent formations in Saudi Arabia show similar patterns for the Late Ordovician but significant differences for the Carboniferous–Permian. The distinct petrographic and geochemical differences between the two formations make it possible to assign stratigraphically uncertain samples.

The high maturity of the Upper Ordovician Enticho Sandstone is probably a consequence of strong chemical weathering in the source area before the glaciation combined with long transport by the glaciers and reworking in a shallow marine environment after the glaciation. The material is possibly sourced from Archean cratons and/or Proterozoic mobile belts in central Gondwana, such as the Congo and Tanzania cratons or the Kibaran, Irumide or Mozambique belts. The Edaga Arbi Glacials have a proximal source, most likely the Arabian–Nubian Shield. These findings support previous models of a large ice sheet covering northern Gondwana in the Late Ordovician, leading to a regional mixture and homogenisation of source material, and a complex pattern of local glaciers in the Carboniferous–Permian.

Acknowledgements

This project was funded by the German Research Foundation (DFG grants HI 643/13-1, ME 3882/4-1). We thank Gerald Hartmann for XRF analysis and Klaus Simon for ICP-MS analysis. Careful and constructive reviews by Carita Augustsson and Martin Keller are greatly appreciated

Appendix. Supplementary data

Supplementary data associated with this article can be found in the online version at http://xxxxxx

References

Aitchison, J., 1982. The Statistical Analysis of Compositional Data. Journal of the Royal Statistical Society. Series B (Methodological) 44, 139–177.
Aitchison, J., 1986. The Statistical Analysis of Compositional Data. Chapman & Hall, London/New York.
Aitchison, J., 2003. A Concise Guide to Compositional Data Analysis, University of Glasgow, Department of Statistics.
Alene, M., Jenkin, G.R.T., Leng, M.J., Darbyshire, D.P.F., 2006. The Tambien Group, Ethiopia: An early Cryogenian (ca. 800–735 Ma) Neoproterozoic sequence in the Arabian–Nubian Shield. Precambrian Research 147, 79–99.
Arkin, Y., Beyth, M., Dow, D.B., Levitte, D., Temesgen, H., Tsegaye, H., 1971. Geological Map of Mekele Area, Sheet ND 37-11, Geological Survey of Ethipia, Addis Abeba, Scale: 1:250,000
Avigad, D., Sandler, A., Kolodner, K., Stern, R., McWilliams, M., Miller, N., Beyth, M., 2005. Mass-production of Cambro–Ordovician quartz-rich sandstone as a consequence of chemical weathering of Pan-African terranes: Environmental

implications. Earth and Planetary Science Letters 240, 818–826.

Bassis, A., Hinderer, M., Meinhold, G., 2016a. New insights into the provenance of Saudi Arabian Palaeozoic sandstones from heavy mineral analysis and single-grain geochemistry. Sedimentary Geology 333, 100–114.

Bassis, A., Hinderer, M., Meinhold, G., 2016b. Petrography and geochemistry of Palaeozoic quartz-rich sandstones from Saudi Arabia: implications for provenance and chemostratigraphy. Arabian Journal of Geosciences 9:400, doi:10.1007/s12517-016-2412-z

Beyth, M., 1972a. Paleozoic-Mesozoic sedimentary basin of the Mekele Outlier, Northern Ethiopia. American Association of Petroleum Geologists Bulletin 56, 2426–2439.

Beyth, M., 1972b. To the geology of central-western Tigre. PhD thesis, Rheinische Friedrich-Wilhelms-Universität Bonn, 159 pp.

Bhatia, M.R., Crook, K.A.W., 1986. Trace element characteristics of graywackes and tectonic setting discrimination of sedimentary basins. Contributions to Mineralogy and Petrology 92, 181–193.

Bussert, R., 2010. Exhumed erosional landforms of the Late Palaeozoic glaciation in northern Ethiopia: Indicators of ice-flow direction, palaeolandscape and regional ice dynamics. Gondwana Research 18, 356–369.

Bussert, R., 2014. Depositional environments during the Late Palaeozoic ice age (LPIA) in northern Ethiopia, NE Africa. Journal of African Earth Sciences 99, 386–407.

Bussert, R., Schrank, E., 2007. Palynological evidence for a latest Carboniferous-Early Permian glaciation in Northern Ethiopia. Journal of African Earth Sciences 49, 201–210.

Bussert, R., Dawit, E.L., 2009. Unexpected diversity: New results on the stratigraphy and sedimentology of Palaeozoic and Mesozoic siliciclastic sediments in Northern Ethiopia. Zentralblatt für Geologie und Paläontologie Teil I(3/4), 181–198.

Chamley, H., Debrabant, P., Foulon, J., d'Argoud, G.G., Latouche, C., Maillet, N., Maillot, H., Sommer, F., 1979. Mineralogy and geochemistry of Cretaceous and Cenozoic Atlantic sediments off the Iberian Peninsula (Site 398, DSDP LEG 47B). In: Laughter, F.H. (Ed.), Leg 47, Part 2 of the cruises of the drilling vessel Glomar Challenger, Vigo, Spain to Brest, France; April-May 1976. Initial Reports of the Deep Sea Drilling Project, Vol. 47 (Part 2), Texas A&M University, Ocean Drilling Program, College Station, Texas, United States, pp. 429–449.

Collins, A.S., Pisarevsky, S.A., 2005. Amalgamating eastern Gondwana: The evolution of the Circum-Indian Orogens. Earth-Science Reviews 71, 229–270.

Dawit, E.L., 2010. Adigrat Sandstone in Northern and Central Ethiopia: Stratigraphy, Facies, Depositional Environments and Palynology. PhD thesis, Technical University Berlin, 166 pp.

Dawit, E.L., 2014. Permian and Triassic microfloral assemblages from the Blue Nile Basin, central Ethiopia. Journal of African Earth Sciences 99, 408–426.

Decker, J., Helmold, K.P., 1985. The effect of grain size on detrital modes: a test of the Gazzi-Dickinson point-counting method – discussion. Journal of Sedimentary Petrology 55, 618–620.

Dott, R.H., 1964. Wacke, graywacke and matrix; what approach to immature sandstone classification? Journal of Sedimentary Petrology 34, 625–632.

Dow, D.B., Beyth, M., Hailu, T., 1971. Palaeozoic glacial rocks recently discovered in northern Ethiopia. Geological Magazine 108, 53–60.

Egozcue, J.J., Barceló-Vidal, C., Martín-Fernández, J.A., Jarauta-Bragulat, E., Díaz-Barrero, J.L., Mateu-Figueras, G., 2011. Elements of Simplicial Linear Algebra and Geometry. In: Pawlowsky-Glahn, V., Buccianti, A. (Eds.), Compositional Data Analysis: Theory and Applications. John Wiley & Sons Ltd, Chichester, West Sussex, UK, pp. 139–157.

Eyles, N., 1993. Earth's glacial record and its tectonic setting. Earth-Science Reviews 35, 1–248.

Fielding, C.R., Frank, T.D., Isbell, J.L., 2008. The late Paleozoic ice age – A review of current understanding and synthesis of global climate patterns. In: Fielding, C.R., Frank, T.D., Isbell, J.L. (Eds.), Resolving the Late Paleozoic ice age in time and space. Geological Society of America, Special Paper 441, pp. 343–354.

Folk, R.L., 1951. A comparison chart for visual percentage estimation. Journal of Sedimentary Petrology 21, 32-33.

Garfunkel, Z., 2002. Early Paleozoic sediments of NE Africa and Arabia: Products of continental-scale erosion, sediment transport and deposition. Israel Journal of Earth Sciences 51, 135–156.

Garland, C.R., 1978. Geology of the Adigrat Area. Ministry of Mines, Energy and Water Resources, Geological Survey of Ethiopia, Memoir 1, Addis Abeba, 51 pp.

Garzanti, E., Andò, S., Vezzoli, G., 2008. Settling equivalence of detrital minerals and grain-size dependence of sediment composition. Earth and Planetary Science Letters 273, 138–151.

Ghienne, J.-F., 2003. Late Ordovician sedimentary environments, glacial cycles, and post-glacial transgression in the Taoudeni Basin, West Africa. Palaeogeography, Palaeoclimatology, Palaeoecology 189, 117–145.

Ghienne, J.-F., Le Heron, D.P., Moreau, J., Denis, M., Deynoux, M., 2007. The Late Ordovician glacial sedimentary system of the North Gondwana platform. In: Hambrey, M.J., Christoffersen, P., Glasser, N.F., Hubbard, B. (Eds.), Glacial Sedimentary Processes and Products. International Association of Sedimentologists Special Publication 39, Malden, USA, Oxford, UK, Victoria, Australia, pp. 295–319.

Harangi, Sz., Downes, H., Kósa, L., Szabó, Cs., Thirlwall, M.F., Mason, P.R.D., Mattey, D., 2001. Almandine Garnet in Calc-alkaline Volcanic Rocks of the Northern Pannonian Basin (Eastern–Central Europe): Geochemistry, Petrogenesis and

Geodynamic Implications. Journal of Petrology 42, 1813–1843.

Ingersoll, R.V., Bullard, T.F., Ford, R.L., Grimm, J.P., Pickle, J.D., Sares, S.W., 1984. The effect of grain size on detrital modes: a test of the Gazzi-Dickinson point-counting method. Journal of Sedimentary Petrology 54, 103–116.

Isbell, J.L., Henry, L.C., Gulbranson, E.L., Limarino, C.O., Fraiser, M.L., Koch, Z.J., Ciccioli, P.L., Dineen, A.A., 2012. Glacial paradoxes during the late Paleozoic ice age: Evaluating the equilibrium line altitude as a control on glaciation. Gondwana Research 22, 1–19.

Johnson, P.R., Andresen, A., Collins, A.S., Fowler, A.R., Fritz, H., Ghebreab, W., Kusky, T., Stern, R.J., 2011. Late Cryogenian–Ediacaran history of the Arabian–Nubian Shield: A review of depositional, plutonic, structural, and tectonic events in the closing stages of the northern East African Orogen. Journal of African Earth Sciences 61, 167–232.

Kazmin, V., 1972. Geological Map of Ethiopia. Geological Survey of Ethiopia, Addis Abeba, Scale: 1:2,000,000.

Kazmin, V., Shifferaw, A., Balcha, T., 1978. The Ethiopian basement: Stratigraphy and Possible Manner of Evolution. Geologische Rundschau 67, 531–546.

Keller, M., Hinderer, M., Al-Ajmi, H., Rausch, R., 2011. Palaeozoic glacial depositional environments of SW Saudi Arabia: process and product, Geological Society, London, Special Publication 354, 129–152.

Keller, M., Lehnert, O., 2010. Ordovician paleokarst and quartz sand: Evidence of volcanically triggered extreme climates? Palaeogeography, Palaeoclimatology, Palaeoecology 296, 297–309.

Knox, R.W.O.B., Franks, S.G., Cocker, J.D., 2007. Stratigraphic evolution of heavy-mineral provenance signatures in the sandstones of the Wajid group (Cambrian to Permian), southwestern Saudi Arabia. GeoArabia 12, 65–96.

Kolodner, K., Avigad, D., McWilliams, M., Wooden, J.L., Weissbrod, T., Feinstein, S., 2006. Provenance of north Gondwana Cambrian–Ordovician sandstone: U–Pb SHRIMP dating of detrital zircons from Israel and Jordan. Geological Magazine 143, 367–391.

Konert, G., Afifi, A.M., Al-Hajri, S.A., Droste, H.J., 2001. Paleozoic stratigraphy and hydrocarbon habitat of the Arabian Plate. GeoArabia 6, 407–442.

Kretz, R., 1983. Symbols of rock-forming minerals. American Mineralogist 68, 277–279.

Kumpulainen, R.A., 2007. The Ordovician glaciation in Eritrea and Ethiopia. In: Hambrey, M.J., Christoffersen, P., Glasser, N.F., Hubbard, B. (Eds.), Glacial Sedimentary Processes and Products. International Association of Sedimentologists Special Publication 39, Malden, USA, Oxford, UK, Victoria, Australia, pp. 321–342.

Kumpulainen, R.A., Uchman, A., Woldehaimanot, B., Kreuser, T., Ghirmay, S., 2006. Trace fossil evidence from the Adigrat Sandstone for an Ordovician glaciation in Eritrea, NE Africa. Journal of African Earth Sciences 45, 408–420.

Le Heron, D.P., Craig, J., 2008. First-order reconstructions of a Late Ordovician Saharan ice sheet. Journal of the Geological Society of London 165, 19–29.
Le Heron, D.P., Craig, J., Etienne, J.L., 2009. Ancient glaciations and hydrocarbon accumulations in North Africa and the Middle East. Earth-Science Reviews 93, 47–76.
Martín-Fernández, J.A., Barceló-Vidal, C., Pawlowsky-Glahn, V., 2003. Dealing with zeros and missing values in compositional data sets using nonparametric imputation. Mathematical Geology 35, 253–278.
McBride, E.F., 1963. A classification of common sandstones. Journal of Sedimentary Petrology 33, 664–669.
McLennan, S.M., 1989. Rare earth elements in sedimentary rocks: influence of provenance and sedimentary processes. In: Lipin, B.R., McKay, G.A. (Eds.), Reviews in Mineralogy 21, The Mineralogical Society of America, Washington D.C., pp. 169–196.
McLennan, S.M. 2001. Relationships between the trace element composition of sedimentary rocks and upper continental crust. Geochemistry, Geophysics, Geosystems 2.
McLennan, S.M., Hemming, S., McDaniel, D.K., Hanson, G.N., 1993. Geochemical approaches to sedimentation, provenance, and tectonics. Geological Society of America, Special Paper 284, 21–40.
Meert, J.G., 2003. A synopsis of events related to the assembly of eastern Gondwana. Tectonophysics 362, 1–40.
Meinhold, G., Morton, A.C., Fanning, C.M., Frei, D., Howard, J.P., Phillips, R.J., Strogen, D., Whitham, A.G., 2011. Evidence from detrital zircons for recycling of Mesoproterozoic and Neoproterozoic crust recorded in Paleozoic and Mesozoic sandstones of southern Libya. Earth and Planetary Science Letters 312, 164–175.
Miller, N.R., Alene, M., Sacchi, R., Stern, R.J., Conti, A., Kröner, A., Zuppi, G., 2003. Significance of the Tambien Group (Tigrai, N. Ethiopia) for Snowball Earth events in the Arabian–Nubian Shield. Precambrian Research 121, 263–283.
Miller, N.R., Stern, R.J., Avigad, D., Beyth, M., Schilman, B., 2009. Cryogenian slate-carbonate sequences of the Tambien Group, Northern Ethiopia (I): Pre-“Sturtian” chemostratigraphy and regional correlations. Precambrian Research 170, 129–156.
Morag, N., Avigad, D., Gerdes, A., Belousova, E., Harlavan, Y., 2011. Detrital zircon Hf isotopic composition indicates long-distance transport of North Gondwana Cambrian-Ordovician sandstones. Geology 39, 955–958.
Morton, A.C., Hallsworth, C., 1994. Identifying the provenance-specific features of detrital heavy mineral assemblages in sandstones. Sedimentary Geology 90, 241–256.
Morton, A.C., Meinhold, G., Howard, J.P., Phillips, R.J., Strogen, D., Abutarruma, Y., Elgadry, M., Thusu, B., Whitham, A.G., 2011. A heavy mineral study of sandstones from the eastern Murzuq Basin, Libya: Constraints on provenance and stratigraphic correlation. Journal of African Earth Sciences 61, 308–330.

Nesbitt, H.W., Young, G.M., 1982. Early Proterozoic climates and plate motions inferred from major element chemistry of lutites. Nature 299, 715–717.

Powers, M.C., 1953. A new roundness scale for sedimentary particles. Journal of Sedimentary Petrology 23, 117-119.

Rollinson, H.R., 1993. Using geochemical data - evaluation, presentation, interpretation. Longman, Harlow, UK.

Rubey, W.W., 1933. Settling velocities of gravel, sand and silt particles. American Journal of Science 25, 325–338.

Sacchi, R., Alene, M., Barbieri, M., Conti, A., 2007. On the Palaeozoic Tillite of the Adigrat Group (Tigrai, Ethiopia). Periodico di Mineralogia 76, 241–251.

Saxena, G.N., Assefa, G., 1983. New evidence on the age of the glacial rocks of northern Ethiopia. Geological Magazine 120, 549–554.

Sharland, P.R., Archer, R., Casey, D.M., Davies, R.B., Hall, S.H., Heward, A.P., Horbury, A.D., Simmons, M.D., 2001. Arabian Plate Sequence Stratigraphy. GeoArabia Special Publication 2, Gulf PetroLink, Bahrain.

Squire, R.J., Campbell, I.H., Allen, C.M., Wilson, C.J.L., 2006. Did the Transgondwanan Supermountain trigger the explosive radiation of animals on Earth? Earth and Planetary Science Letters 250, 116–133.

Stern, R.J., 1994. Arc assembly and continental collision in the Neoproterozoic East African Orogen: Implications for the consolidation of Gondwanaland. Annual Review of Earth and Planetary Sciences 22, 319–351.

Stern, R.J., Ali, K.A., Abdelsalam, M.G., Wilde, S.A., Zhou, Q., 2012. U–Pb zircon geochronology of the eastern part of the Southern Ethiopian Shield. Precambrian Research 206–207, 159–167.

Stow, D.A.V., 2005. Sedimentary Rocks in the Field: A Colour Guide. CRC Press Taylor & Francis Group, Boca Raton, USA.

Taylor, S.R., McLennan, S.M., 1985. The Continental Crust: Its Composition and Evolution. Blackwell Scientific Publication, Oxford, UK.

Tefera, M., Chernet, T., Haro, W., 1996. Explanation of the geological map of Ethiopia. T.F.D.R.o. Ethiopia Ministry of Mines and Energy Bulletin 3.

Torsvik, T.H., Cocks, L.R.M., 2013. Gondwana from top to base in space and time. Gondwana Research 24, 999–1030.

Tsige, L., Hailu, F., 2007. Geological Map of the Bure Area, Ministry of Mines and Energy, Geological Survey of Ethiopia Memoir 18, Addis Abeba.

Verma, S.P., Armstrong-Altrin, J.S., 2013. New multi-dimensional diagrams for tectonic discrimination of siliciclastic sediments and their application to Precambrian basins. Chemical Geology 355, 117–133.

Verma, S.P., Armstrong-Altrin, J.S., 2016. Geochemical discrimination of siliciclastic sediments from active and passive margin settings. Sedimentary Geology 332, 1–12.

von Eynatten, H., Tolosana-Delgado, R., Karius, V., 2012. Sediment generation in modern glacial settings: Grain-size and source-

rock control on sediment composition. Sedimentary Geology 280, 80–92.
Whitney, D.L., Evans, B.W., 2010. Abbreviations for names of rock-forming minerals. American Mineralogist 95, 185–187.
Zuffa, G.G., 1985. Optical analyses of arenites: influence of methodology on compositional results. In: Zuffa, G.G. (Ed.), Provenance of Arenites. NATO ASI Series, Series C: Mathematical and Physical Science 148, 165–189.

Tables

Table 1. Samples, corresponding locations, and geographic coordinates (WGS84). The stratigraphic assignment is based on biostratigraphic evidence (B) or lithofacies characteristics (LF) in the outcrop, or it is uncertain (U).

Table 2. Results of petrographic point-counting analysis of thin sections. Values given in %. Qz_m = monocrystalline quartz, Qz_{mu} = monocrystalline quartz with undulose extinction, Qz_p = polycrystalline quartz (subgrain formation), Qz_{micr} = microcrystalline quartz, Pl = plagioclase, Kfs = potassium feldspar, Lp = plutonic lithic fragment, Lv = volcanic lithic fragment (includes metavolcanic clasts, since oriented texture is rarely visible but metamorphic overprint is probable), Ls = sedimentary lithic fragments, Lms = metasedimentary lithic fragments, Lmi = metamorphic igneous lithic fragment, other = minor components such as accessories, unid. = unidentified, e.g., strongly altered. Mineral abbreviations of accessories after Kretz (1983) and Whitney and Evans (2010). Ap = apatite, Cal = calcite, Chl = chlorite, Grt = garnet, Ms = muscovite, Op = opaque, Px = pyroxene, Sil = sillimanite, St = staurolite, Tur = tourmaline, Zrn = zircon. Carbonate cement: 0 = not present, + = up to 5%, ++ = 20–25%. GS = grain size. Sorting: -- = very poor, - = poor, 0 = moderate, + = good, ++ = very good. Roundness: -- = angular, - = subangular, 0 = subrounded, + = rounded, ++ = well rounded.

Figure captions

Fig. 1. Eastern Africa and Arabia with occurrences of Precambrian rocks and major tectonic units. The outline of Ethiopia and the study regions are indicated in blue.

Fig. 2. Geological maps of the study areas showing the sampling locations. Numbers next to the sampling locations correspond to those in Table 1. (a) Northern Ethiopia (modified after Arkin et al., 1971; Garland, 1978; Bussert, 2014). (b) Blue Nile region (modified after Tsige and Hailu, 2007; Dawit, 2014). The term "Fincha Sandstone" is taken from Dawit (2014).

Fig. 3. Field photographs. (a) Sandstone lens above tillite with muddy matrix and rounded clasts of various composition at the base of the Edaga Arbi Glacials. (b) Dropstones in rhythmically laminated sandstone and silt- to claystone in Edaga Arbi Glacials. (c) Striated

boulder in tillite at the base of Edaga Arbi Glacials. (d) Rhythmic mud drapes on cross-beds in marine part of the Enticho Sandstone indicating intertidal environment. (e) Herringbone cross-lamination in marine part of Enticho Sandstone indicating tidal environment. (f) Alternation of graval bends and sandstone in glaciogenic part of Enticho Sandstone. (g) Tillite at the base of glaciogenic Enticho Sandstone. (h) Soft-sediment deformation structures in sandstone underlying tillite in the basal part of Enticho Sandstone.

Fig. 4. Sandstone classification diagram after McBride (1963). Q = quartz, F = feldspar, L = lithic fragments (thin section point-counting).

Fig. 5. Thin section photomicrographs of the Edaga Arbi Glacials and the marine and glaciogenic units of the Enticho Sandstone. Qz = quartz, Pl = plagioclase, Kfs = potassium feldspar, Lp = plutonic lithic fragment, Lv = (meta)volcanic lithic fragment, St = staurolite, Ky = kyanite, Zrn = zircon (mineral abbreviations after Kretz, 1983; Whitney and Evans, 2010). PPL = plane-polarised light, XPL = cross-polarised light.

Fig. 6. Selected major and trace element concentrations normalised to the average upper continental crust (UCC; normalising values from McLennan, 2001) are shown on the left side. Rare earth element concentrations normalised to average CI chondrites (normalising values from Taylor and McLennan, 1985) are shown on the right side.

Fig. 7. Compositional biplots of (a) the first two principal components of a principal component analysis (PCA) based on the clr-transformed concentrations of the major and trace elements considered in Fig. 6 with the sum of LREE and HREE, (b) the first and second and (c) the first and third principal components of a PCA based on the clr-transformed concentrations of a subset of the elements considered in Fig. 6, which is assumed to be less affected by diagenesis and leaching.

Fig. 8. Tectonic setting discrimination diagrams after Verma and Armstrong-Altrin (2013, 2016). (a) Discriminant functions (DF) based on major oxides (SiO_2, TiO_2, Al_2O_3, Fe_2O_3, MnO, MgO, CaO, Na_2O, K_2O, P_2O_5; Verma and Armstrong-Altrin, 2013). (b) Discriminant function based on major oxides and selected trace elements (SiO_2, TiO_2, Al_2O_3, Fe_2O_3, MnO, MgO, CaO, Na_2O, K_2O, P_2O_5, Cr, Nb, Ni, V, Y, Zr; Verma and Armstrong-Altrin, 2016).

Fig. 9. Th/Sc versus Zr/Sc diagram after McLennan et al. (1993). (a) Samples analysed in this study, stratigraphically equivalent units from Saudi Arabia (Bassis et al., 2016b), boulders in tillite of the Edaga Arbi Glacials (granitoid, diorite/gabbro, basalt and gneiss) and local basement (granite, metabasite and metasedimentary rocks; this study). (b) Samples analysed in this study grouped by their geographic position.

Fig. 10. Compositional biplots of (a) the first and second and (b) the first and third principal components of a principal component analysis (PCA) based on the clr-transformed concentrations of the major and trace elements in Fig. 7 (b, c) comparing the samples analysed in this study with stratigraphically equivalent samples from Bassis et al. (2016b), local basement samples and boulders in tillite of the Edaga Arbi Glacials (this study). Co is left out, because it was not measured by Bassis et al. (2016b). Carb. = Carboniferous, Perm. = Permian, Ord. = Ordovician.

Fig. 11. Summary of the main findings of this study for the two Gondwana glaciations in Ethiopia. Gondwana palaeogeography and south pole positions from Torsvik and Cocks (2013). Ice sheet locations and transport directions for the Late Ordovician are after Ghienne et al. (2007), Le Heron and Craig (2008), and Torsvik and Cocks (2013), and for the Carboniferous–Permian they are after Bussert and Schrank (2007), Fielding et al. (2008), and Isbell et al. (2012).

Figure 1

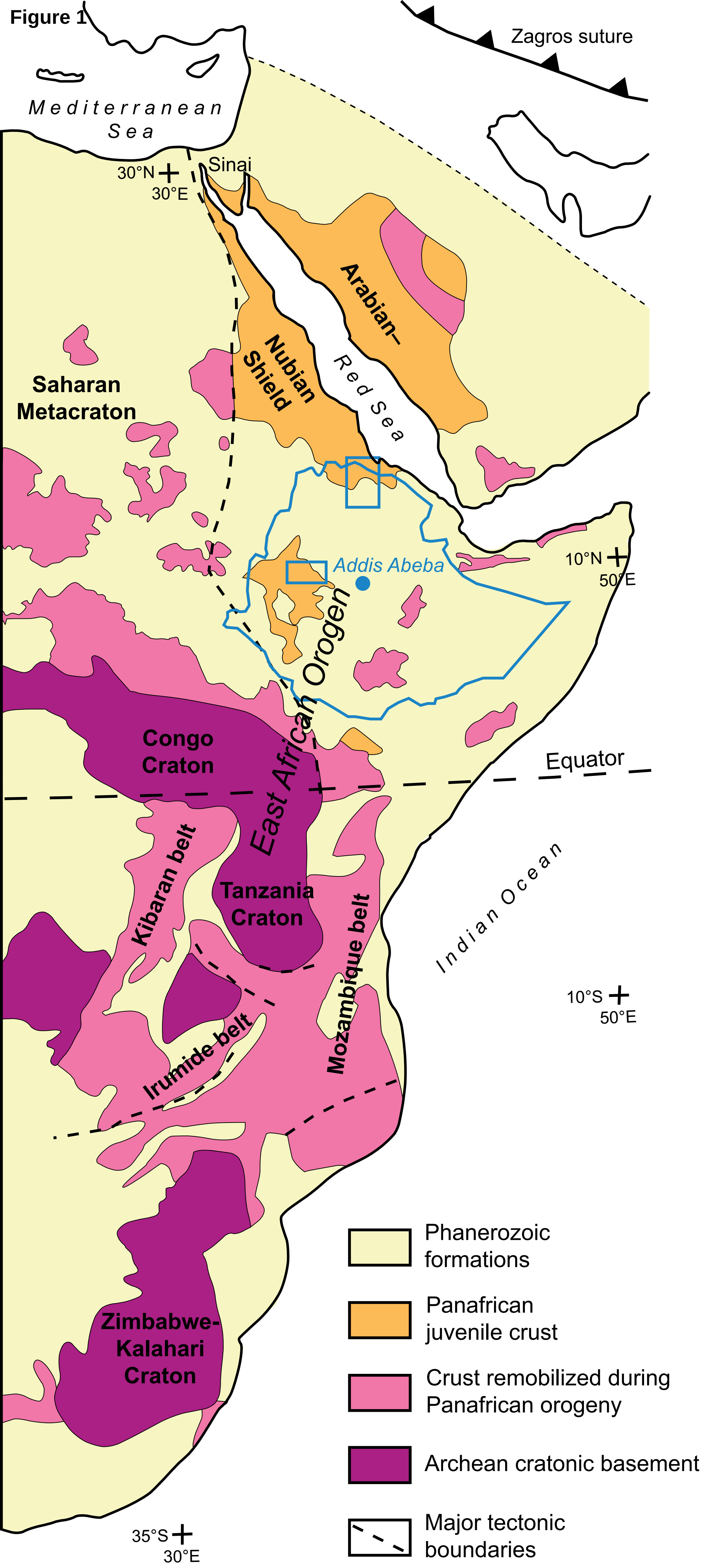

Zagros suture
Mediterranean Sea
Sinai
30°N
30°E
Arabian–
Nubian Shield
Red Sea
Saharan Metacraton
Addis Abeba
10°N
50°E
East African Orogen
Congo Craton
Equator
Kibaran belt
Tanzania Craton
Mozambique belt
Indian Ocean
10°S
50°E
Irumide belt
Zimbabwe-Kalahari Craton
35°S
30°E
Phanerozoic formations
Panafrican juvenile crust
Crust remobilized during Panafrican orogeny
Archean cratonic basement
Major tectonic boundaries

Figure 2

Click here to download high resolution image

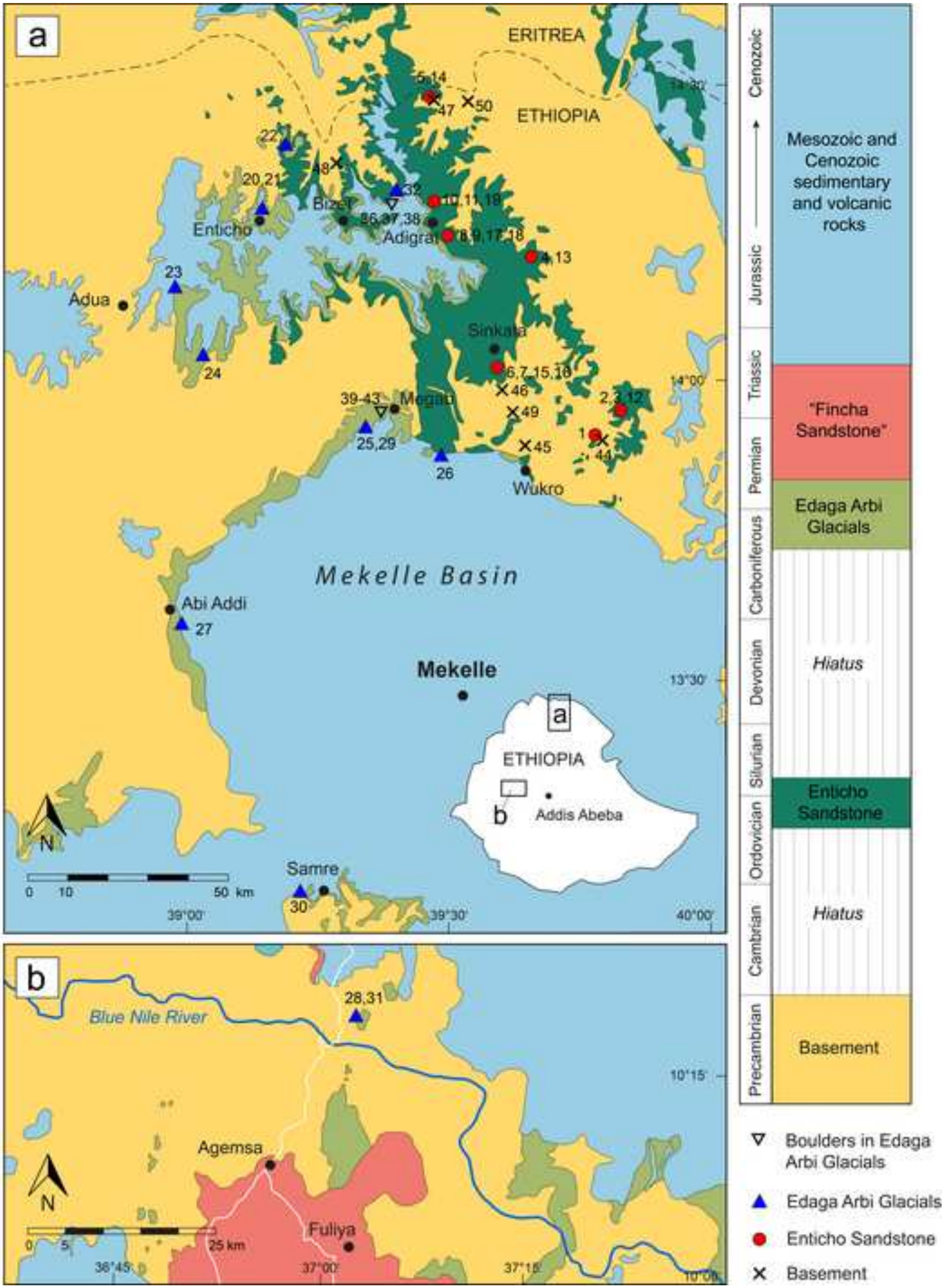

Figure 3

Click here to download high resolution image

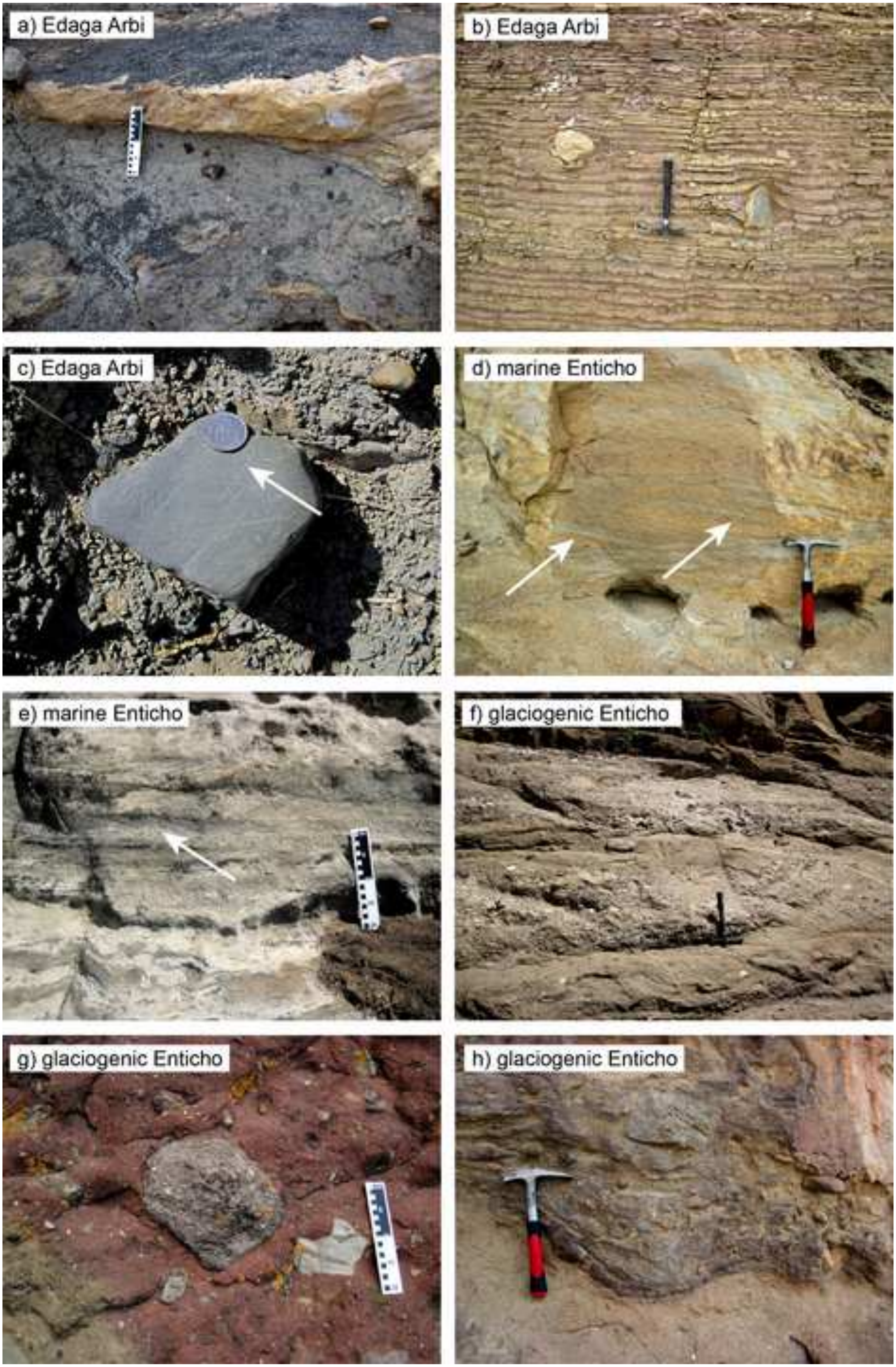

Figure 4

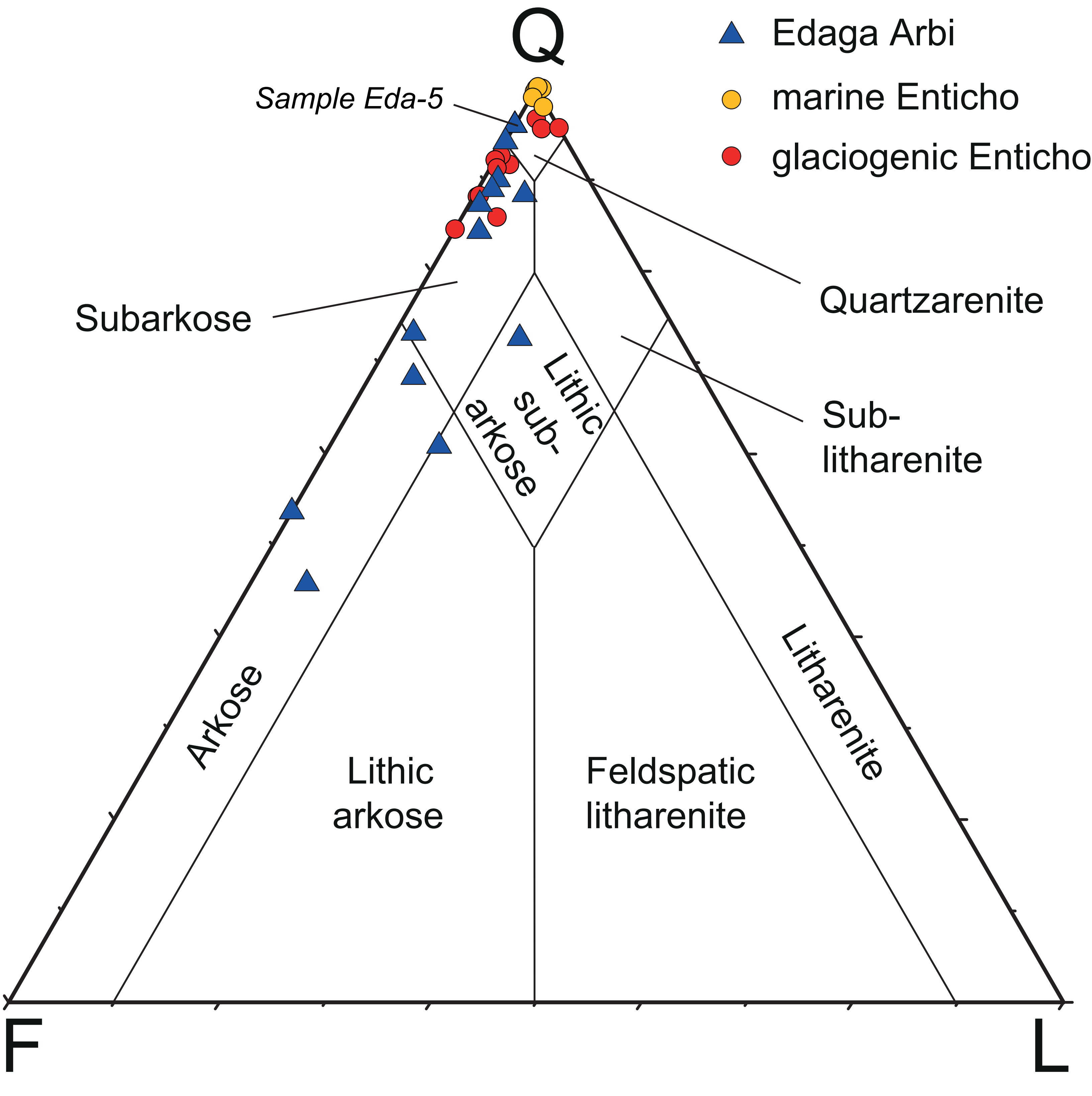

Q
F
L
Edaga Arbi
marine Enticho
glaciogenic Enticho
Sample Eda-5
Subarkose
Quartzarenite
Sub-
litharenite
Lithic
sub-
arkose
Arkose
Lithic
arkose
Feldspatic
litharenite
Litharenite

Figure 5

Click here to download high resolution image

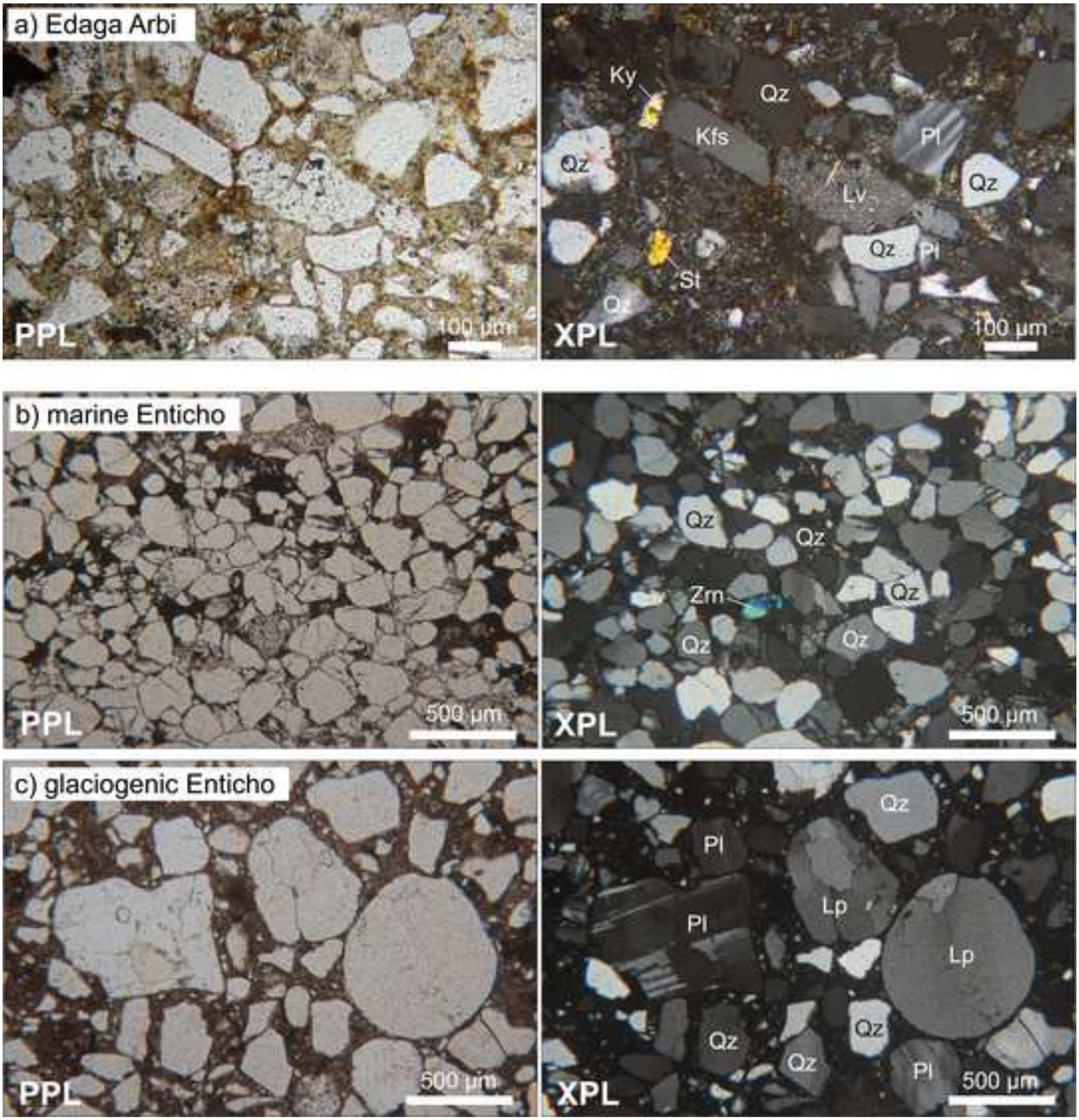

Figure 6

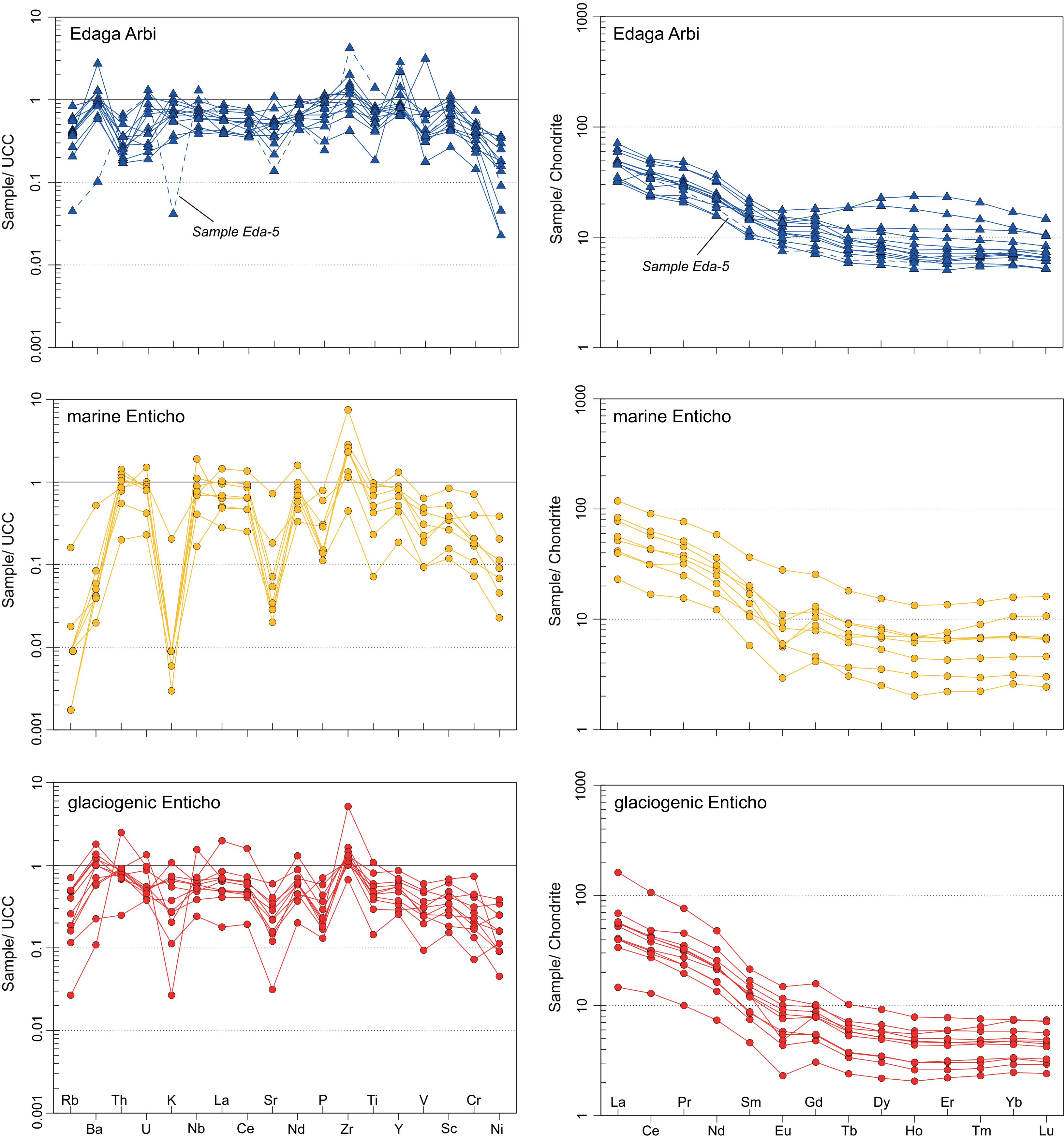

Edaga Arbi
Sample Eda-5
Sample/ UCC
Sample/ Chondrite
marine Enticho
glaciogenic Enticho
10
1
0.1
0.01
0.001
1000
100
Rb
Ba
Th
U
K
Nb
La
Ce
Sr
Nd
P
Zr
Ti
Y
V
Sc
Cr
Ni
La
Ce
Pr
Nd
Sm
Eu
Gd
Tb
Dy
Ho
Er
Tm
Yb
Lu

Figure 7

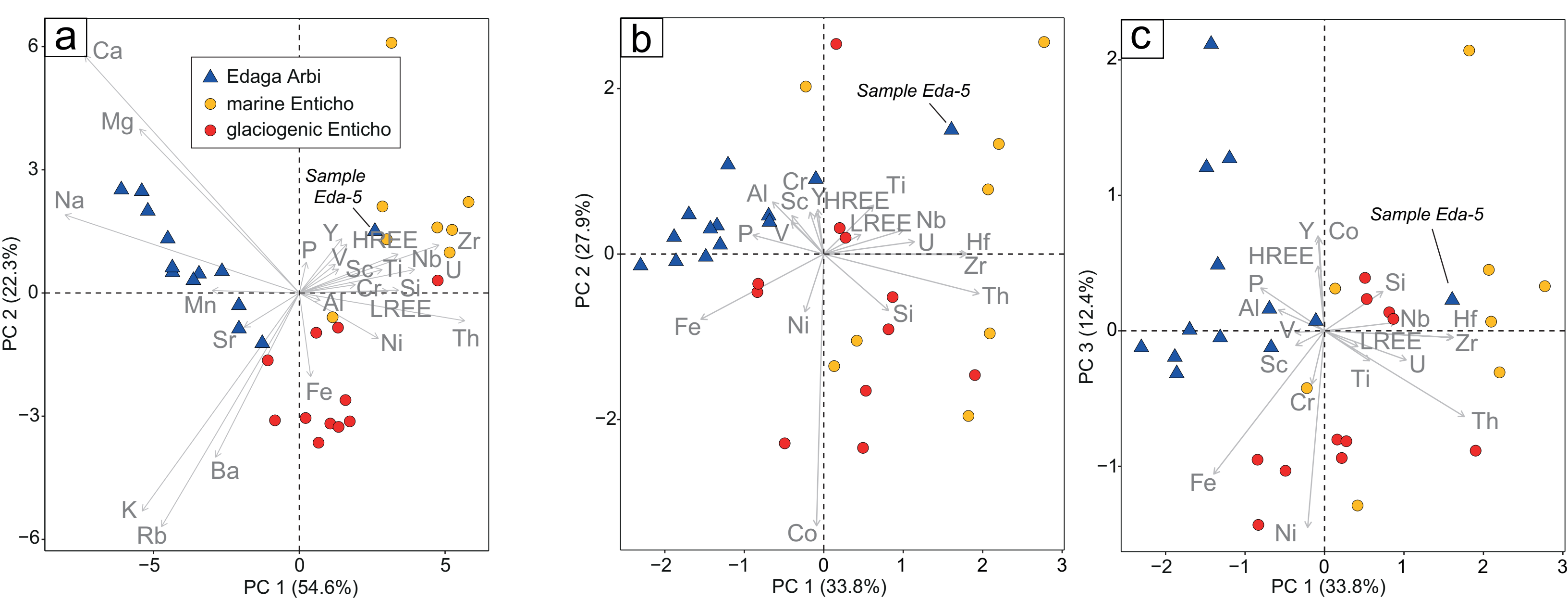

a
Edaga Arbi
marine Enticho
glaciogenic Enticho
Sample Eda-5
PC 1 (54.6%)
PC 2 (22.3%)
b
Sample Eda-5
PC 1 (33.8%)
PC 2 (27.9%)
c
Sample Eda-5
PC 1 (33.8%)
PC 3 (12.4%)

Figure 8

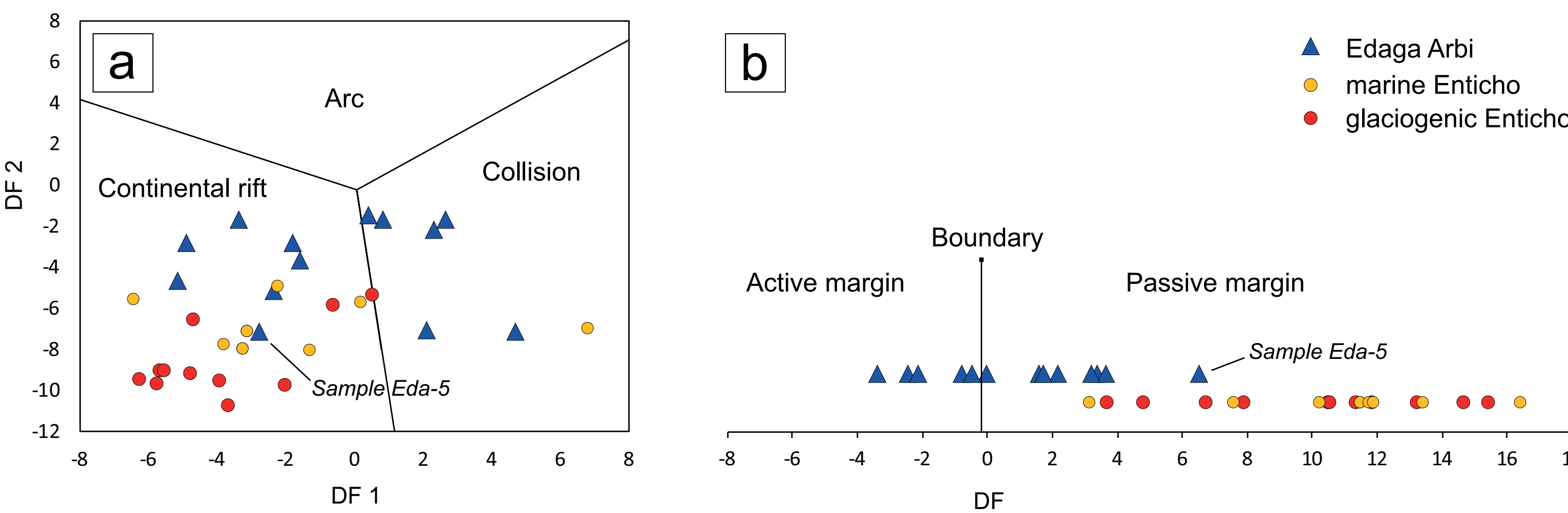
a
Arc
Continental rift
Collision
Sample Eda-5
DF 2
DF 1
b
Edaga Arbi
marine Enticho
glaciogenic Enticho
Boundary
Active margin
Passive margin
Sample Eda-5
DF

Figure 9

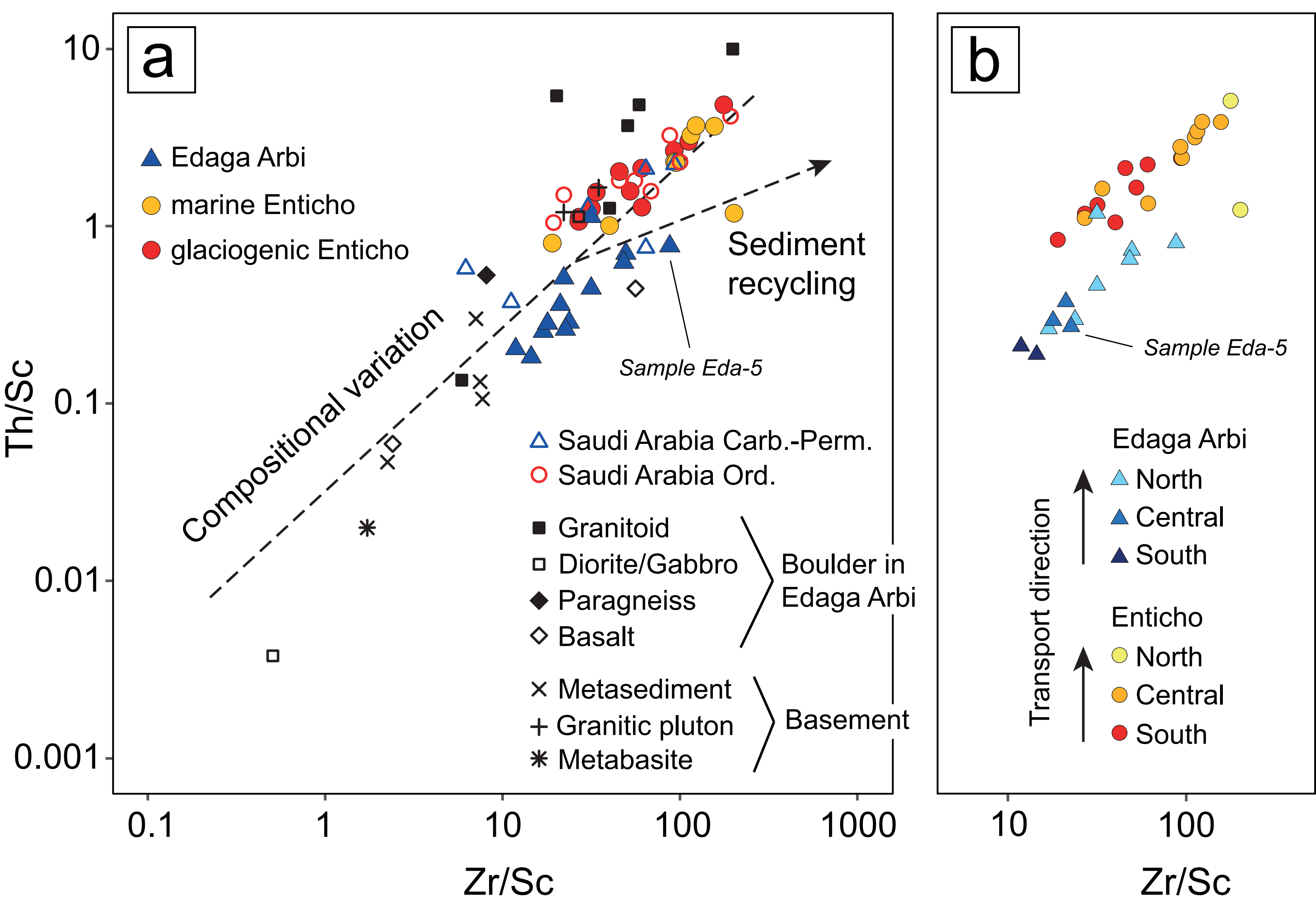
a
b
Edaga Arbi
marine Enticho
glaciogenic Enticho
Compositional variation
Sediment recycling
Sample Eda-5
Saudi Arabia Carb.-Perm.
Saudi Arabia Ord.
Granitoid
Diorite/Gabbro
Paragneiss
Basalt
Boulder in Edaga Arbi
Metasediment
Granitic pluton
Metabasite
Basement
Th/Sc
Zr/Sc
10
1
0.1
0.01
0.001
0.1
1
10
100
1000
Sample Eda-5
Edaga Arbi
North
Central
South
Enticho
North
Central
South
Transport direction
Zr/Sc
10
100

Figure 10

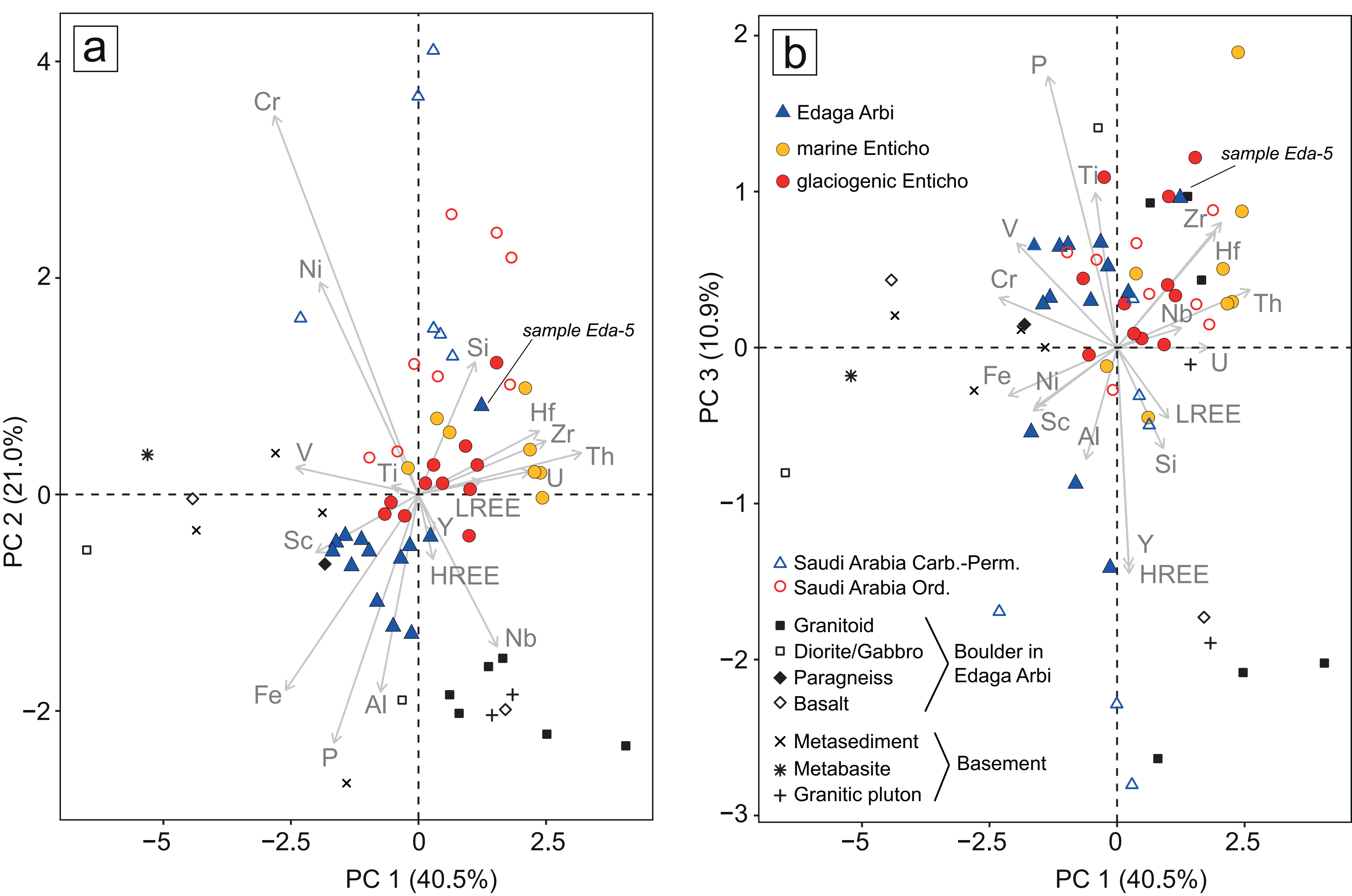

a
b
PC 1 (40.5%)
PC 2 (21.0%)
PC 3 (10.9%)
sample Eda-5
Cr
Ni
V
Ti
Si
Hf
Zr
Th
U
LREE
Y
HREE
Nb
Sc
Fe
Al
P
Edaga Arbi
marine Enticho
glaciogenic Enticho
Saudi Arabia Carb.-Perm.
Saudi Arabia Ord.
Granitoid
Diorite/Gabbro
Paragneiss
Basalt
Boulder in Edaga Arbi
Metasediment
Metabasite
Granitic pluton
Basement

Figure 11

Maturity → Transport Weathering → Source area

Geochemical signature → Source area

		Maturity	Transport	Weathering	Geochemical signature	Source area
Carboni-ferous–Permian	**Edaga Arbi Glacials**	low	short	little	more juvenile crustal material	local (ANS)
Ordovician–Silurian	**Enticho Sandstone**	high	far	strong	old, differentiated crustal material	distant (inner Gondwana)

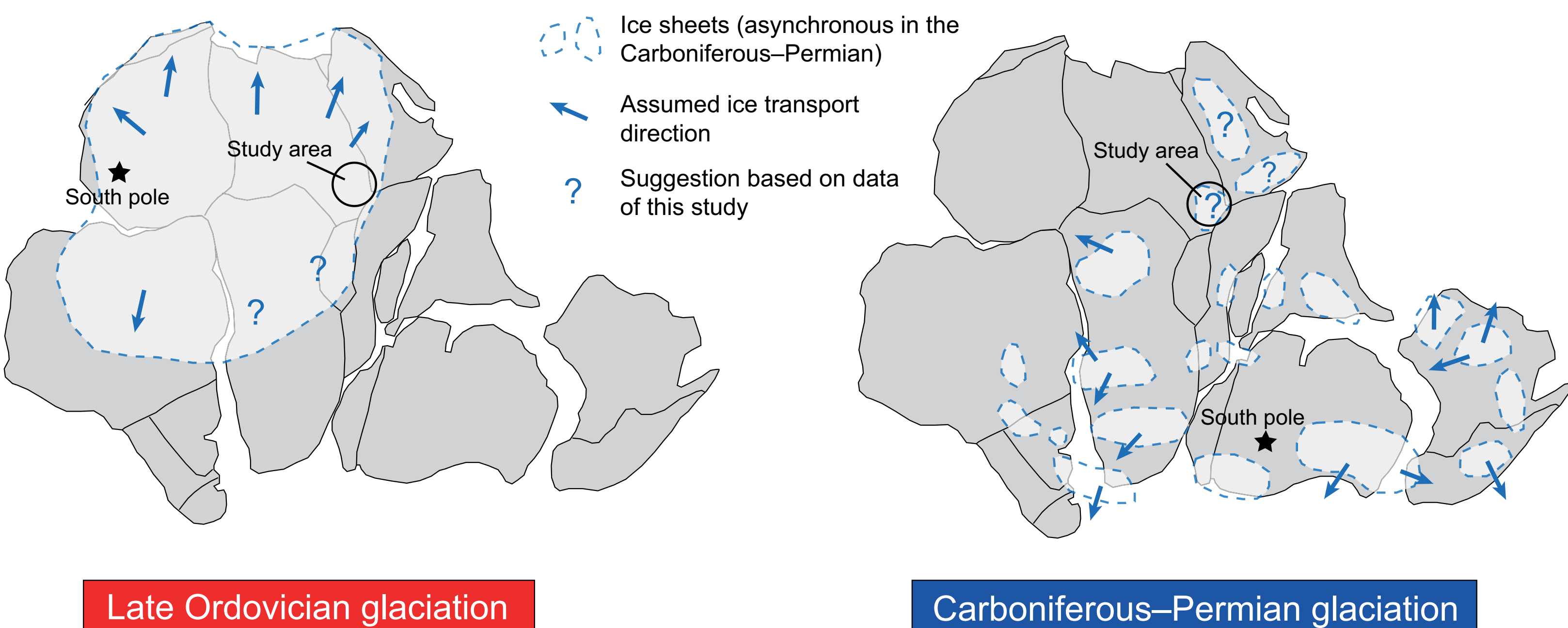

Table 1

#	Sample	Formation	Age	Location	North(°)	East(°)	Position within Fm.	Facies/ Lithology	Strati-graphic assignment
1	Enti-4	Enticho	Upper Ordovician	Atsbi south	13.83465	039.71262	Base	Tillite matrix	U
2	Enti-5	Enticho	Upper Ordovician	Atsbi north	13.88828	039.74783	Base	Glacial	B
3	Enti-7	Enticho	Upper Ordovician	Atsbi north	13.88842	039.74259	Base	Glacial	B
4	Enti-9	Enticho	Upper Ordovician	Wollwello	14.22037	039.65014	Base	Glacial	B
5	Enti-13	Enticho	Upper Ordovician	Zalambassa	14.49275	039.41911	Base	Glacial	LF
6	S1	Enticho	Upper Ordovician	Sinkata	13.96861	039.61167	Base	Glacial	B
7	S2	Enticho	Upper Ordovician	Sinkata	13.96861	039.61167	Base	Glacial	B
8	Nib-1	Enticho	Upper Ordovician	Adigrat south	14.25194	039.48972	Base	Glacial	B
9	Nib-2	Enticho	Upper Ordovician	Adigrat south	14.25194	039.48972	Base	Glacial	B
10	North-1	Enticho	Upper Ordovician	Adigrat north	14.31333	039.46000	Base	Glacial	B
11	North-2	Enticho	Upper Ordovician	Adigrat north	14.31333	039.46000	Base	Glacial	B
12	Enti-6	Enticho	Upper Ordovician	Atsbi north	13.88842	039.74827	Top	Marine	B
13	Enti-10	Enticho	Upper Ordovician	Wollwello	14.21839	039.64994	Top	Marine	B
14	Enti-12	Enticho	Upper Ordovician	Zalambassa	14.49627	039.41911	Top	Marine	LF
15	S3	Enticho	Upper Ordovician	Sinkata	13.97056	039.61111	Top	Marine	B
16	S4	Enticho	Upper Ordovician	Sinkata	13.97056	039.61111	Top	Marine	B
17	Nib-3	Enticho	Upper Ordovician	Adigrat south	14.25222	039.49583	Top	Marine	B
18	Nib-4	Enticho	Upper Ordovician	Adigrat south	14.25222	039.49583	Top	Marine	B
19	North-3	Enticho	Upper Ordovician	Adigrat north	14.31944	039.45889	Top	Marine	B
20	Eda-2	Edaga Arbi	Carboniferous-Permian	Enticho	14.28166	039.14725	Base	Tillite matrix	B
21	Eda-3	Edaga Arbi	Carboniferous-Permian	Enticho	14.27929	039.14836	Base	Sand lens	U
22	Eda-4	Edaga Arbi	Carboniferous-Permian	Edaga Robi	14.38906	039.18161	Base	Tillite matrix	U
23	Eda-6	Edaga Arbi	Carboniferous-Permian	Edaga Arbi west	14.05667	039.07095	Base	Sand lens	LF
24	Eda-8	Edaga Arbi	Carboniferous-Permian	Megab south	13.90944	039.32301	Base	Sand lens	B
25	Eda-10	Edaga Arbi	Carboniferous-Permian	Dugum	13.84957	039.49003	Base	Sand lens	LF
26	Eda-11	Edaga Arbi	Carboniferous-Permian	Abi Addi	13.61842	039.00042	Base	Sand lens	LF
27	Hu-1	Edaga Arbi	Carboniferous-Permian	Bure, Blue Nile	10.31057	037.05068	Base	Sand lens	LF
28	Eda-9	Edaga Arbi	Carboniferous-Permian	Megab south	13.90915	039.32235	Top	Sand lens	B
29	Eda-12	Edaga Arbi	Carboniferous-Permian	Samre	13.17844	039.19745	Top	Sand lens	B
30	Hu-2	Edaga Arbi	Carboniferous-Permian	Bure, Blue Nile	10.31057	037.05068	Top	Sand lens	LF
31	Eda-1	Edaga Arbi	Carboniferous-Permian	Adigrat west	14.31171	039.40472	Uncertain	Tillite matrix	LF
32	Eda-5	Uncertain	Uncertain	Adwa east	14.19102	038.93957	Uncertain	Sand lens	U
33	Bas-1		Unknown	Megab	13.93496	039.36520		Metabasite	
34	Bas-2		Unknown	Megab	13.93496	039.36520		(Meta)basite	
35	Gn-1		Unknown	Megab	13.93496	039.36520		Paragneiss	
36	Gr-3	Boulders	Unknown	Adigrat west	14.31171	039.40472		Granitoid	
37	Gr-4	in	Unknown	Adigrat west	14.31171	039.40472		Granitoid	
38	Gr-5	Edaga	Unknown	Adigrat west	14.31171	039.40472		Granitoid	
39	Gr-6	Arbi	Unknown	Megab	13.93496	039.36520		Granitoid	
40	Gr-7	tillite	Unknown	Megab	13.93496	039.36520		Granitoid	
41	Gr-8		Unknown	Megab	13.93496	039.36520		Granitoid	
42	Gr-9		Unknown	Megab	13.93496	039.36520		Diorite/Gabbro	
43	Gr-10		Unknown	Megab	13.93496	039.36520		Diorite/Gabbro	
44	Neop-1	Basement	Neoproterozoic	Atsbi south	13.83374	039.71132		Metagreywacke	
45	Neop-2	Basement	Neoproterozoic	Negash	13.83561	039.61442		Metatillite	
46	Neop-3	Basement	Neoproterozoic	near Negash	13.94186	039.59876		Metabasite	
47	Neop-4	Basement	Neoproterozoic	Zalambassa	14.49276	039.41899		Metapelite	
48	Neop-5	Basement	Neoproterozoic	Road Debre Damo – Enticho	14.37729	039.27883		Metagreywacke	
49	Gr-1	Basement pluton	Neoproterozoic	Negash highschool	13.89164	039.60517		Granitoid	
50	Gr-2	Basement pluton	Neoproterozoic	Sebea	14.46629	039.48225		Granitoid	

Table 2

Sample	Formation	Qz_m [%]	Qz_{mu} [%]	Qz_p [%]	Qz_{micr} [%]	Pl [%]	Kfs [%]	Lp [%]	Lv [%]	Ls [%]	Lms [%]	Lmi [%]	Other [%]	Unid. [%]	Counts	Accessories	Carbo-nate cement	Matrix [%]	GS (mm)	Sor-ting	Round-ness
Enti-4	Enticho	69.3	5.7	9.3	1.0	5.0	5.7	2.3	0.0	1.0	0.0	0.0	0.7	0.0	300	Tur, Zrn	0	40	0.05-4	--	-
Enti-5	Enticho	69.0	9.7	8.7	0.0	4.0	7.3	0.3	0.0	0.0	0.0	0.0	0.0	1.0	300		0	40	0.05-4	--	-- to ++
Enti-7	Enticho	63.7	14.3	5.7	0.7	5.3	10.0	0.0	0.0	0.0	0.0	0.0	0.0	0.3	300		0	10	0.1-1	0	+
Enti-9	Enticho	68.3	15.7	6.7	0.0	4.0	4.0	0.0	0.0	0.7	0.0	0.0	0.7	0.0	300	Mica, Px (?)	0	35	0.05-2; 0.1-1 (layers)	-	- to +
Enti-13	Enticho	62.3	14.7	18.3	0.7	0.3	1.3	0.7	0.0	1.0	0.0	0.0	0.3	0.3	300	Zrn	0	5	0.1-1	0	- to +
S1	Enticho	48.3	31.0	12.3	0.0	1.3	5.3	1.7	0.0	0.0	0.0	0.0	0.0	0.0	300		0	< 5	0.1-5	--	+ to ++
S2	Enticho	68.7	15.3	6.3	0.0	3.3	4.3	0.0	0.0	0.0	0.0	0.0	0.7	1.3	300		0	< 5	0.1-1	-	- to ++
Nib-1	Enticho	80.3	8.7	4.0	0.7	0.3	1.3	0.7	2.0	0.0	0.0	0.0	0.7	1.3	300	Tur	0	< 5	0.1-1	0	- to +
Nib-2	Enticho	73.3	9.0	5.7	0.0	4.3	7.0	0.3	0.0	0.0	0.0	0.0	0.0	0.3	300	Zrn	0	25	0.05-1.2	-	- to ++
North-1	Enticho	70.0	21.3	1.3	0.0	2.0	5.0	0.3	0.0	0.0	0.0	0.0	0.0	0.0	300		0	5	0.1-0.5	+	- to +
North-2	Enticho	73.3	15.7	6.7	0.0	0.0	0.0	0.0	0.0	4.3	0.0	0.0	0.0	0.0	300		0	50	0.05-7	-	- to ++
Enti-6	Enticho	78.0	17.7	3.3	0.3	0.0	0.7	0.0	0.0	0.0	0.0	0.0	0.0	0.0	300		0	5	0.1-1	+	- to ++
Enti-10	Enticho	85.0	9.3	2.3	0.0	0.3	0.0	0.0	0.0	0.0	0.0	0.0	3.0	0.0	300	Op+, Px?, Chl, Ap	0	< 5	0.1	++	-
Enti-12	Enticho	87.3	8.3	3.7	0.0	0.0	0.3	0.0	0.0	0.0	0.0	0.0	0.3	0.0	300	Grt	0	10	0.1-1.2	+	+
S3	Enticho	77.3	12.0	9.3	0.7	0.0	0.0	0.0	0.0	0.0	0.0	0.0	0.7	0.0	300	Chl, Op	0	< 5	0.1-1	-	- to +
S4	Enticho	79.0	14.7	6.3	0.0	0.0	0.0	0.0	0.0	0.0	0.0	0.0	0.0	0.0	300		0	55	0.1-1	0	+
Nib-3	Enticho	84.7	7.7	5.3	0.0	0.3	0.0	1.7	0.0	0.0	0.0	0.0	0.3	0.0	300	Zrn	0	< 5	0.1-1	0	+
Nib-4	Enticho	70.3	26.3	2.7	0.0	0.0	0.0	0.3	0.0	0.0	0.0	0.0	0.3	0.0	300		0	< 5	0.1-0.8	+	+
North-3	Enticho	81.7	18.0	0.3	0.0	0.0	0.0	0.0	0.0	0.0	0.0	0.0	0.0	0.0	300		0	< 5	0.1-0.6	+	+ to ++
Eda-2	Edaga Arbi	63.0	14.3	0.3	3.7	3.3	3.0	0.0	2.7	1.7	0.0	0.0	6.7	1.3	300	Op+, Grt, Zrn+, Cal, Ms	+	25	0.05-0.2	+	+
Eda-3	Edaga Arbi	76.3	10.7	0.3	0.0	3.3	8.3	0.7	0.0	0.0	0.3	0.0	0.0	0.0	300		+	< 5	0.05-0.3	0	0 to +
Eda-4	Edaga Arbi	68.7	20.0	0.0	0.0	4.0	5.7	0.3	0.7	0.0	0.3	0.0	0.0	0.3	300	Grt	0	15	0.05-0.3	0	0 to +
Eda-5	Edaga Arbi	84.3	10.3	0.7	0.0	0.0	4.0	0.0	0.0	0.0	0.0	0.0	0.3	0.3	300	Zrn+	0	35	0.05-0.5	0	-- to +
Eda-6	Edaga Arbi	60.7	3.7	1.0	0.3	5.3	21.0	0.0	0.3	3.7	0.0	0.0	3.0	1.0	300	Zrn+, Grt, Sil, St	++	< 5	0.1-0.3	+	-
Eda-8	Edaga Arbi	76.0	10.0	0.0	1.3	5.0	3.3	0.0	0.0	1.3	0.0	0.0	0.0	3.0	300		++	25	0.05-0.1	+	+
Eda-10	Edaga Arbi	52.3	4.7	3.0	0.7	6.3	22.3	6.0	1.7	1.0	1.3	0.3	0.3	0.0	300		+	20	0.1-0.7	0	- to 0
Eda-11	Edaga Arbi	70.7	2.3	2.7	5.3	6.3	6.3	0.0	1.0	1.3	0.0	0.0	1.3	2.7	300	Op, Chl	++	40	0.05-0.5	0	-
Hu-1	Edaga Arbi	39.3	5.7	0.7	0.0	12.0	36.7	4.3	0.0	1.0	0.0	0.0	0.3	0.0	300	Op	+	5	0.1-3	--	- to 0
Eda-9	Edaga Arbi	67.7	14.7	2.0	2.0	1.7	3.7	0.0	0.0	0.0	0.0	0.0	7.7	0.7	300	Chl+, Ms	0	35	0.05-0.1	++	+
Eda-12	Edaga Arbi	61.3	5.3	1.3	1.3	7.3	16.3	0.0	1.7	0.0	0.0	0.0	1.0	4.3	300	Zrn, Grt, Cal	0	40	0.05-0.2	0	- to 0
Hu-2	Edaga Arbi	46.0	7.3	0.0	0.0	9.0	37.0	0.0	0.0	0.0	0.0	0.0	0.7	0.0	300	Tur, Grt	0	10	0.1-0.3	+	0 to +
Eda-1	Edaga Arbi	58.3	7.3	3.0	1.3	6.7	8.0	7.0	2.7	1.7	0.3	0.0	1.3	2.3	300	Op, Grt	++	< 5	0.1-0.3	0	+